Disruption of protein rhamnosylation affects the *Sporothrix schenckii*-host interaction

Alma K. Tamez-Castrellón [a], Samantha L. van der Beek [b], Luz A. López-Ramírez [a], Iván Martínez-Duncker [c], Nancy E. Lozoya-Pérez [a], Nina M. van Sorge [b,1], Héctor M. Mora-Montes [a,*]

[a] *Departamento de Biología, División de Ciencias Naturales y Exactas, Campus Guanajuato, Universidad de Guanajuato, Noria Alta s/n, col. Noria Alta, C.P. 36050 Guanajuato, Gto., Mexico*
[b] *University Medical Center Utrecht, Medical Microbiology, Heidelberglaan 100, 3584 CX Utrecht, The Netherlands*
[c] *Laboratorio de Glicobiología Humana y Diagnóstico Molecular, Centro de Investigación en Dinámica Celular, Instituto de Investigación en Ciencias Básicas y Aplicadas, Universidad Autónoma del Estado de Morelos, Cuernavaca Mor. 62209, Mexico*

A B S T R A C T

Sporotrichosis is a fungal disease caused by the members of the *Sporothrix* pathogenic clade, and one of the etiological agents is *Sporothrix schenckii.* The cell wall of this organism has been previously analyzed and thus far is known to contain an inner layer composed of chitin and β-glucans, and an outer layer of glycoproteins, which are decorated with mannose and rhamnose-containing oligosaccharides. The L-rhamnose biosynthesis pathway is common in bacteria but rare in members of the Fungi kingdom. Therefore, in this study, we aimed to disrupt this metabolic route to assess the contribution of rhamnose during the *S. schenckii*-host interaction. We identified and silenced in *S. schenckii* a functional ortholog of the bacterial *rmlD* gene, which encodes for an essential reductase for the synthesis of nucleotide-activated L-rhamnose. *RmlD* silencing did not affect fungal growth or morphology but decreased cell wall rhamnose content. Compensatory, the β-1,3-glucan levels increased and were more exposed at the cell surface. Moreover, when incubated with human peripheral blood mononuclear cells, the *RmlD* silenced mutants differentially stimulated cytokine production when compared with the wild-type strain, reducing TNFα and IL-6 levels and increasing IL-1 β and IL-10 production. Upon incubation with human monocyte-derived macrophages, the silenced strains were more efficiently phagocytosed than the wild-type strain. In both cases, our data suggest that rhamnose-based oligosaccharides are ligands that interact with TLR4. Finally, our findings showed that cell wall rhamnose is required for the *S. schenckii* virulence in the *G. mellonella* model of infection.

1. Introduction

Sporotrichosis is an acute or chronic granulomatous subcutaneous mycosis that occurs in humans and other mammals. These infections are caused by members of the pathogenic clade of the *Sporothrix* genus, which contains the species *Sporothrix schenckii, Sporothrix brasiliensis, Sporothrix globosa,* and *Sporothrix luriei* (de Beer et al., 2016). The disease has a worldwide distribution and several clinical manifestations, ranging from the most common acute and chronic cutaneous and subcutaneous lesions to more serious infections involving the lymph nodules, fascia, cartilage, muscle, and bones (Chakrabarti et al., 2015, Lopes-Bezerra et al., 2018a). The etiological agents are widely distributed in the environment, although regionalisms can be observed for some of the species, and thus far, it is considered to be a unique infection caused by a dimorphic fungus with a substantial zoonotic transmission (Chakrabarti et al., 2015).

Similar to the other members of the pathogenic clade, *S. schenckii* is a dimorphic organism, and the mycelial form is considered the

saprophytic morphology found when growing in the environment. In contrast, the yeast-like morphotype is frequently found when invading the host tissues (Mora-Montes et al., 2015, Lopes-Bezerra et al., 2018a).

The fungal cell wall is a dynamic structure that confers protection to stress, controls permeability, is essential to cell viability, morphogenesis, and pathogenesis (Díaz-Jiménez et al., 2012). Moreover, the cell wall contains molecules that induce and modulate innate and adaptive immune responses (Netea et al., 2006, Netea et al., 2008, Latgé et al., 2017, Martinez-Alvarez et al., 2017, Lopes-Bezerra et al., 2018a). The *S. schenckii* cell wall is composed of chitin, β-1,6-, β-1,4-, and β-1,3-glucans that form the inner layer; whilst the cell surface or outer layer is composed mostly of peptidorhamnomannan, which is a complex of molecules with a wide molecular weight range, containing 12.2% of proteins, 57% of mannose and 33.5% of rhamnose (Lloyd and Bitoon, 1971, Martinez-Alvarez et al., 2017, Lopes-Bezerra et al., 2018b). Similar to *S. schenckii*, the fungal pathogen *Pseudallescheria boydii* contains rhamnomannan in its cell wall (Pinto et al., 2001), which activates macrophages in a TLR4-dependent manner (Figueiredo et al., 2010) and is crucial for adhesion to mammalian cells (Pinto et al., 2004). These rhamnomannans from both species are immunogenic structures that are recognized by antibodies (Lopes-Bezerra, 2011). In bacteria, the rhamnose-containing cell wall polysaccharides have been described to have an important role in virulence, increasing adherence and immune evasion, changes in the structure of these polysaccharides caused attenuation of virulence in a mouse model of peritonitis, this reduction in the virulence correlated with enhanced phagocytic uptake and clearance by neutrophils (Teng et al., 2002, Mistou et al., 2016).

Rhamnose is incorporated in many glycoproteins, exopolysaccharides, and other components of the fungal cell wall in *Rhynchosporium secales*, *Cephalotheca purpurea*, *Cephalotheca reniformis*, *Penicillium chrysogenum,* and *Ophiostoma ulmi* (Martinez et al., 2012). In both *Magnaporthe grisea* and *Botryotinia fuckeliana,* rhamnose synthesis is carried out using UDP-glucose as a precursor, using two enzymes, one of wich has a double enzymatic activity (Fig. 1) (Martinez et al., 2012). The functional orthologs for the protein-encoding genes have also been reported in *Botrytis cinerea* (Ma et al., 2017). In bacteria, the rhamnose synthesis involves four enzymes with unique enzymatic activities that convert the precursor glucose to dTDP-L-rhamnose, and the main difference with the fungal system is the epimerization and reduction steps that are carried out by individual enzymes, RmlC and RmlD, respectively (Fig. 1) (Graninger et al., 1999, Giraud and Naismith, 2000).

To gain insights into the role of rhamnose-containing molecules during the *S. schenckii*-host interaction, we silenced *RmlD* and performed a phenotypical characterization of the mutant cells. In particular, we analyzed the changes in the cell wall composition, the interaction with human peripheral blood mononuclear cells (PBMCs), with human monocyte-derived macrophages, and assessed the virulence in *Galleria mellonella* larvae.

2. Material and methods

2.1. Strains and culture media

Strains used and generated here are listed in Table 1. Fungal cells were maintained at 28 °C in YPD medium, pH 4.5 (1% [w/v] yeast extract, 2% [w/v] gelatin peptone, and 3% [w/v] dextrose).
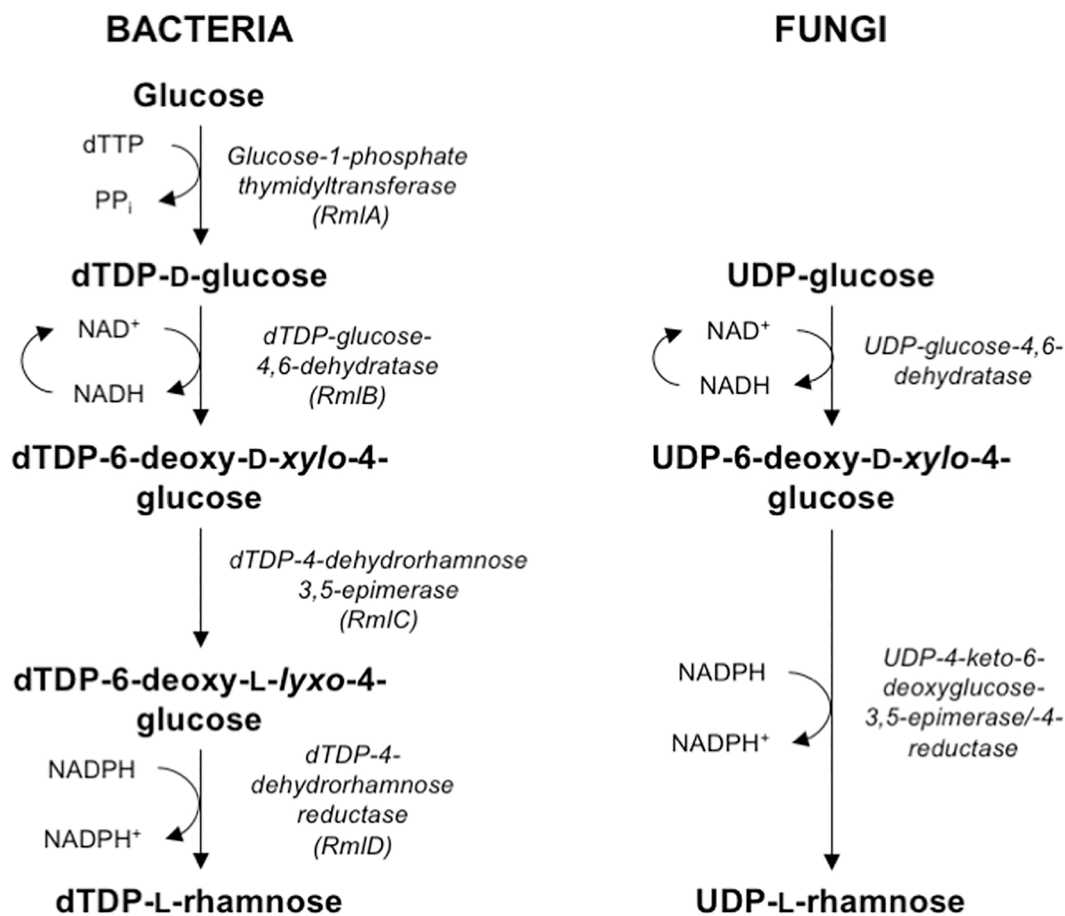
Fig. 1. Synthesis of nucleotide-bound rhamnose in bacteria and fungi. In bacteria the biosyntethic pathway involves four different enzymes (RmlA, RmlB, RmlC and RmlD) and starts with glucose as precursor. The main differences in fungi are the precursor, UDP-glucose in this case, and that the last two steps in the synthesis are carried out by a single enzyme with bifunctional activity (epimerase and reductase).

Table 1

Strains used in this work.

Strain	Organism	Genotype	Reference
Xc	*Streptococcus mutans*	Serotype C wild-type strain	(Koga et al., 1989)
SMU Δ*rmlD*	*Streptococcus mutans*	Xc Δ*rmlD*::*erm*	(van der Beek et al., 2015)
SMU D*rmlD* + pSs*RmlD*	*Streptococcus mutans*	Xc Δ*rmlD*::*erm* transformed with pSs*rmlD*	This work
1099–18 ATCC MYA 4821	*Sporothrix schenckii*	Wild-type	(Castro et al., 2013)
HSS29	*Sporothrix schenckii*	1099–18 ATCC MYA 4821 transformed with pBGgHg	This work
HSS30	*Sporothrix schenckii*	1099–18 ATCC MYA 4821 transformed with pBGgHg	This work
HSS20	*Sporothrix schenckii*	1099–18 ATCC MYA 4821 transformed with pBGgHg-RmlD	This work
HSS21	*Sporothrix schenckii*	1099–18 ATCC MYA 4821 transformed with pBGgHg-RmlD	This work
HSS22	*Sporothrix schenckii*	1099–18 ATCC MYA 4821 transformed with pBGgHg-RmlD	This work
HSS23	*Sporothrix schenckii*	1099–18 ATCC MYA 4821 transformed with pBGgHg-RmlD	This work
HSS24	*Sporothrix schenckii*	1099–18 ATCC MYA 4821 transformed with pBGgHg-RmlD	This work
HSS25	*Sporothrix schenckii*	1099–18 ATCC MYA 4821 transformed with pBGgHg-RmlD	This work

Agrobacterium tumefaciens AGL-1 was maintained at 28 °C in Luria-Bertani medium (0.5 [w/v] yeast extract, 1% [w/v] gelatin peptone, and 1% [w/v] NaCl). When selection required, the medium was supplemented with 100 μg mL^{-1} ampicillin and 100 μg mL^{-1} kanamycin. For conidia, cells were grown on solid YPD medium, pH 4.5, at 28 °C for 7 days, and then harvested by surface scratching, as described (Martinez-Alvarez et al., 2017). For hyphal growth, conidia were incubated in YPD broth, pH 4.5, at 28 °C and 120 rpm for 48 h, and harvested by filtering, using a vacuum system and a 5-μm nylon membrane (Monodur®). For yeast-like cells, conidia were incubated in YPD broth, pH 7.8 for 7 days at 37 °C and 120 rpm, as described, and harvested by centrifuging at 5000 × *g* for 5 min at 4 °C (Martinez-Alvarez et al., 2017). In both cases, cells were washed three times with deionized water and kept at −20 °C until used. Heat inactivation of cells was carried out at 60 °C for 2 h, (Martinez-Alvarez et al., 2017) and confirmation of the viability loss was performed on YPD plates, pH 4.5, incubated at 28 °C for 5 days. Upon *Agrobacterium*-mediated transformation, *S. schenckii* cells were selected on YPD plates, pH 4.5 added with 400 mg mL^{-1} hygromycin B, and incubated at 28 °C for 5 days (Lozoya-Pérez et al., 2018, Lozoya-Perez et al., 2019). *Streptococcus mutans* Xc was cultured in Todd-Hewitt Broth (THB; Oxoid) or on THB agar at 37 °C with 5% CO$_2$. When required, THB was supplemented with 10 μg mL^{-1} erythromycin or 3 μg mL^{-1} chloramphenicol.

2.2. Heterologous complementation of Streptococcus mutans ΔrmlD

The heterologous expression was performed following a methodology previously described by van der Beek et al. (2015). Briefly, the *S. schenckii RmlD* open reading frame was cloned into XbaI and BamHI sites of the vector pDC123 (Chaffin and Rubens, 1998), generating pSs*RmlD*, which was used to transform *S. mutans* Xc wild-type and selected by the conferred resistance to chloramphenicol. The presence of the plasmid inside the bacteria was confirmed by PCR. The bacterial *rmlD* gene was knocked out by precise in-frame allelic replacement of *rmlD* with an erythromycin resistance gene in *S. mutans* + pSs*rmlD* (van der Beek

et al., 2015). For this, the disruption cassette was constructed as follows. A fragment of 700 bp immediately upstream of *rmlD* was amplified with the primers 5′-CGCAGCAAGCAGTTACGTGATTTGTTGAAG and 5′-GTTTTGAGAATATTTTATATTTTTGTTCATTATTTTTTTCTCCTTTAAAAAGCTTTATTACTATTACC, and a fragment of 674 bp immediately downstream of *rmlD* was amplified with the primers 5′-AGTTATCTAT-TATTTAACGGGAGGAAATAATATTTTAGCAAAGAAGGACAGGTTTAAACC-3′ and 5′-CTGAAGGTGATAAATCCGTGCCATA-3′ (underlined sequences correspond to 30 bp to the 5′ and 3′ ends of the *erm* gene, respectively). The upstream and downstream PCR fragments were fused by PCR with the 738 bp amplicon of the *erm* gene, amplified from the pDCerm plasmid (Jeng et al., 2003). The resultant *rmlD* disruption cassette was used to transform *S. mutans* + pSs*RmlD* and transformants were selected by the double resistance to erythromycin and chloramphenicol. PCR analysis and sequencing were used to confirm the native *rmlD* disruption. As a result, *S. mutans* Δ*rmlD* + pSs*RmlD* was generated.

For electron microscopy, overnight cultures were diluted and grown to the mid-log phase, cells harvested by centrifuging, and samples were washed, fixed, and dehydrated as described previously (Garufi et al., 2012). Then, cells were mounted onto 12.5 mm specimen stubs (Agar Scientific) and coated with gold to 1 nm using a Quorum Q150R S sputter coater at 20 mA. Visual examination was performed with a Phenom PRO desktop scanning electron microscope (Phenom-World BV), operated with an acceleration voltage of 10 kV.

2.3. Sporothrix schenckii RmlD silencing

Fungal genomic DNA was isolated as described elsewhere (Robledo-Ortiz et al., 2012) and used, along with the primer pair 5′-CTCGA-GATGTCCGACAAACACGTACTCG and 5′-AAGCTTAATGTTGCGGGCAGCACA (underlined sequences are added recognition sites for XhoI and HindIII, respectively) to amplify 315 bp fragment of the 5′ region of the *RmlD* open reading frame. The amplicon was cloned into the pSilent-1 XhoI and HindIII sites (Nakayashiki et al., 2005) generating the construction pSilent-1-*RmlD*-sense. The antisense fragment was amplified by PCR using a primer pair with the same sequence as the one used for amplification of the sense region, but with recognitions sites in the 5′ ends for StuI and BglII for forward and reverse primers, respectively. The resulting amplicon was cloned into the StuI and BglII sites of pSilent-1-*RmlD*-sense, generating pSilent-1-*RmlD*-sense-antisense. This construction, along with the primer pair 5′-CTGCAGATGCCAGTTGTTCCCAGTGATC and 5′-GAGCTCCCTCTAAACAAGTGTACCTGTGCATT (underlined sequences are added recognition sites for PstI and SacI, respectively), were used to amplify by PCR a 2814 bp amplicon that spans from the *Aspergillus nidulans TrpC* promoter to the *A. nidulans trpC* terminator, including the sense-intron-antisense region for *RmlD* (Lozoya-Perez et al., 2019). The amplicon was cloned into the PstI and SacI sites of the binary vector pBGgHg (Chen et al., 2000), generating pBGgHg-*RmlD*. This construction was used to transform *A. tumefaciens* AGL-1, and then cells were incubated in minimal medium (0.34 M K$_2$HPO$_4$, 0.16 M NaH$_2$PO$_4$, 0.37 M NH$_4$Cl, 0.24 MgSO$_4$, 0.04 M KCl, 1.8 mM CaCl$_2$, FeSO$_4$ 0.18 mM, pH 7.0 adjusted with 1 N HCl) supplemented with 200 μM acetosyringone (Sigma) for 4.5 h at 28 °C and 250 rpm (Lozoya-Pérez et al., 2018). Aliquots of 100 μL bacterial suspension and 100 μL of conidia at 1 × 10^6 conidia mL^{-1} were mixed and incubated for 72 h at 28 °C on a cellophane disk on top of YPD agar. Then, the cellophane was placed on YPD, pH 4.5 added with 400 mg mL^{-1} hygromycin B and 200 μM cefotaxime, and incubated for 72 h at 28 °C. The transformant cells were subjected to five monoconidial passages in YPD, pH 4.5, and three events of dimorphism induction in YPD, pH 7.8. In all cases, the media were added with 400 mg mL^{-1} hygromycin B for transformants selection.

2.4. Analysis of gene expression and insertional events in mutant strains

The insertion of the binary plasmid within the fungal genome was confirmed by PCR, using the primer pair 5′-

GGCGACCTCGTATTGGGAATC and 5′-CTATTCCTTTGCCCTCGGAC-GAG-3′, as previously described (Lozoya-Perez et al., 2019). The forward primer aligns in the *pdg* promoter and the reverse primer inside the *hph* marker. Total RNA was extracted as described elsewhere (Robledo-Ortiz et al., 2012), cDNA synthesized and purified as reported (Trujillo-Esquivel et al., 2016, Trujillo-Esquivel et al., 2017), quantified in a NanoDrop 2000 (Thermo Scientific), and used in qPCR reactions in a thermocycler StepOne Plus (Life Technologies). The PCR reactions contained the SYBR Green PCR Master Mix (Life Technologies) and the primer pair 5′-GTCCGACAAACACGTACTCG and 5′-GGGTCCTTG TCGACCTTGT that generated an amplicon of 243 bp from the 5′ end of the *RmlD* open reading frame. To estimate the number of the binary plasmid insertional events the same strategy was used, but genomic DNA was used instead of cDNA. In both RT-qPCR and qPCR data were analyzed with the StepOne software V 2.2 (Life Technologies) and the $2^{-\Delta\Delta Ct}$ method (Livak and Schmittgen, 2001). The encoding gene for the ribosomal protein L6 was used for data normalization and was amplified with the primer pair 5′-ATTGCGACATCAGAGAAGG and 5′-TCGACCTTCTTGATGTTGG, as reported (Trujillo-Esquivel et al., 2017); while the parental strain 1099–18 ATCC MYA 4821 was considered as the reference condition.

2.5. Cell wall analysis

Cells homogenates from yeast-like cells were mechanically prepared in a Braun homogenizer as described elsewhere (Mora-Montes et al., 2010b). Cell walls were resuspended in deionized water and centrifuged for 10 min at 20 000 × g and 4 °C, the supernatant discarded and the pellet washed additionally five times with deionized water. Then, cell walls were subjected to removal of intracellular contaminant components by serial incubations with hot SDS, β-mercaptoethanol, and NaCl, and then hydrolyzed with 2 M trifluoroacetic acid (Sigma-Aldrich), as described. (Mora-Montes et al., 2007) Acid-hydrolyzed samples were analyzed by High-Performance Anion-Exchange Chromatography with Pulsed Amperometric Detection (HPAEC-PAD) with a Dionex system (Thermo Fisher Scientific), using separation conditions reported elsewhere (Estrada-Mata et al., 2015). For cell wall protein concentration, cleansed walls were alkali-hydrolyzed as reported (Mora-Montes et al., 2007), before quantification using the Pierce BCA Protein Assay (Thermo Fisher Scientific).

To estimate the ability to bind Alcian blue, yeast-like cells were grown to mid-log phase, then pelleted by centrifuging, washed twice with deionized water, and the cell concentration adjusted at an OD_{600} of 0.2 in deionized water. Aliquots of 1 mL were used to interact with 30 μg mL^{-1} Alcian blue (Sigma-Aldrich) and analyzed as described (Hobson et al., 2004). The cell wall porosity to polycations was calculated as described previously (De Nobel et al., 1990), incubating cells with either 30 μg mL^{-1} poly-L-lysine (MW 30–70 kDa, Sigma-Aldrich) or 30 μg mL^{-1} diethylaminoethyl-dextran (MW 500 kDa, Sigma-Aldrich).

2.6. Analysis of cell wall N-linked and O-linked glycans

To trim *O*-linked glycans 1×10^9 yeast-like cells were resuspended in 1 N NaOH and gently shook for 18 h at room temperature. For *N*-linked glycans removal, aliquots containing 1×10^9 yeast-like cells were incubated for 20 h at 37 °C with 25 U endoglycosidase H (New England Biolabs) (Lozoya-Perez et al., 2019). In both cases, cells were pellet by centrifuging, and the supernatants were collected, lyophilized, and stored at −20 °C until used. Total sugar content was quantified with the phenol–sulfuric-acid method (Dubois et al., 1956), while acid hydrolysis and monosaccharide separation was performed by HPAEC-PAD as described. (Mora-Montes et al., 2012).

2.7. Chitin and β1,3-glucan staining

For chitin labeling, yeast-like cells were incubated with 500 μg mL^{-1}

fluorescein isothiocyanate conjugated-wheat germ agglutinin (WGA-FITC; Sigma-Aldrich) for 60 min at room temperature, as reported. (Mora-Montes et al., 2011); whilst β1,3-glucan was labeled by incubating cells with 5 μg mL^{-1} IgG Fc-Dectin-1 chimera (Graham et al., 2006) for 40 min at room temperature, followed by an additional incubation with 1 μg mL^{-1} donkey anti-Fc IgG-FITC (Sigma-Aldrich) for 40 min at room temperature (Marakalala et al., 2013). Samples were examined under fluorescence microscopy in a Zeiss Axioscope-40 microscope and an Axiocam MRc camera. The fluorescence quantification of 300 cells was collected using the software Adobe Photoshop™ CS6 and the formula: [(total of green pixels-background green pixels) × 100]/total pixels (Pérez-García et al., 2016).

2.8. Ethics statement

The Ethics Committee from Universidad de Guanajuato approved the inclusion of primary human cells in this study (Ref. 17082011). Only healthy adult volunteers that received information about the study and signed the informed consent were enrolled. The inclusion of insects in this project was approved by the same institutional Committee (Ref. CIBIUG-P12-2018).

2.9. Stimulation of cytokine production by human peripheral blood mononuclear cells

PBMCs were isolated from human EDTA-treated venous blood, which upon withdrawn was mixed with Histopaque-1077 (Sigma-Aldrich) and subjected to differential centrifugation, as previously reported (Endres et al., 1988). The fungus-immune cell interactions were performed in round-bottom 96-well microplates, using live yeast-like cells (Martinez-Alvarez et al., 2017). Each well contained 100 μL 1 × 10^5 yeast-like cells and 100 μL 5 × 10^5 PBMCs in RPMI 1640 Dutch modification (added with 2 mM glutamine, 0.1 mM pyruvate and 0.05 mg mL^{-1} gentamycin; all reagents from Sigma-Aldrich). The microplates were incubated for 24 h at 37 °C with 5% (v/v) CO_2, centrifuged for 10 min at 3000 × g at 4 °C, the supernatants saved, and kept at −20 °C until used. When indicated, the PBMCs suspensions were pre-incubated for 1 h at 37 °C and 5% (v/v) CO_2 with 200 μg mL^{-1} laminarin (Sigma-Aldrich), 10 μg mL^{-1} anti-TLR2 (eBioscience), or 10 μg mL^{-1} anti-TLR4 (Santa Cruz Biotechnology), before interaction with yeast-like cells. Preincubations with Isotype matched, 10 μg mL^{-1} irrelevant IgG$_1$ antibody (Santa Cruz Biotechnology) were used as a control for TLR4 blocking; while preincubations with 10 μg mL^{-1} IgG$_{2α}$κ (eBioscience) were included to control TLR2 blocking assays (Martinez-Alvarez et al., 2017). To avoid any bias for the presence of bacterial lipopolysaccharide, all the fungus-PBMCs interactions were added with 5 μg mL^{-1} polymyxin B (Sigma-Aldrich) (Martinez-Alvarez et al., 2017), despite were negative for this bacterial wall component, assessed with a *Limulus* amebocyte lysate (Sigma-Aldrich). The interleukin 1β (IL-1β) concentration was determined in the collected supernatants by ELISA, using a DuoSet ELISA Development kit (R&D Systems); whereas the tumor necrosis factor-alpha (TNFα), interleukin 6 (IL-6), and interleukin 10 (IL-10) were quantified by ELISA with Standard ABTS ELISA Development kits (Peprotech). In all cases, mock interactions with only human PBMCs were included as controls.

2.10. Analysis of phagocytosis by human monocyte-derived macrophages

Upon isolation as described in the previous section, human PMBCs were differentiated to macrophages using recombinant human granulocyte–macrophage colony-stimulating factor (Sigma-Aldrich) (Pérez-García et al., 2016). Before interactions, yeast-like cells were washed twice with PBS and incubated with 1 mg mL^{-1} Acridine Orange (Sigma-Aldrich) as described (Hernández-Chávez et al., 2019), and then washed twice with PBS and cell concentration adjusted at 3 × 10^7 yeast-like cells mL^{-1}. The interactions were performed with a macrophage-yeast ratio

of 1:6, in 6-well plates, and a final volume of 800 μL DMEM medium (Sigma-Aldrich) per well (Lozoya-Perez et al., 2019). After 2 h of incubation at 37 °C and 5% (v/v) CO$_2$, macrophages were washed twice with chilled PBS and stained with 1.25 mg mL^{-1} Trypan Blue, as an external fluorescence quencher, as described (González-Hernández et al., 2017). The cell–cell interactions were analyzed by flow cytometry in a FACS-Canto II equipped with a FACSDiva acquisition system (Becton Dickinson, Franklin Lakes, NJ, USA). A total of 50,000 events were collected per sample or condition, gating for immune cells (González-Hernández et al., 2017, Hernández-Chávez et al., 2018, Lozoya-Perez et al., 2019). Fluorescent signals were obtained using the FL1 (green) and FL2 (red) channels, previously compensated with non-stained macrophages. All the interactions were performed in presence of polymyxin B 5 μg mL^{-1}, and when required, preincubations of macrophages with 200 μg mL^{-1} laminarin (Sigma-Aldrich), 200 μg mL^{-1} L-rhamnose (Sigma-Aldrich), 10 μg mL^{-1} anti-TLR2 (eBioscience), 10 μg mL^{-1} anti-TLR4 (Santa Cruz Biotechnology), 10 μg mL^{-1} irrelevant IgG$_1$ antibody (Santa Cruz Biotechnology), or 10 μg mL^{-1} irrelevant IgG$_2$aκ (eBioscience) were performed for 1 h at 37 °C and 5% (v/v) CO$_2$. Cells emitting fluorescence in the green channel were considered in the early stage of phagocytosis, cells emitting in both the green and red channels were considered to be in the intermediate stage of this immune event; while those only emitting signals in the red channel were considered to be in the late stage of the phagocytic process (Hernández-Chávez et al., 2018, Lozoya-Perez et al., 2019).

2.11. Analysis of fungal virulence in Galleria mellonella

The *G. mellonella* larvae were from an in-house colony previously established (Clavijo-Giraldo et al., 2016) and were raised and fed ad libitum on corn bran and honey diet (1 kg corn bran, 150 g rice meal, 250 mL bee honey, and 70 mL glycerin) (García-Carnero et al., 2020). Only larvae with irritability, absence of body melanization, and a length of 1.2–1.5 cm were included in the host-fungus interaction assays (Clavijo-Giraldo et al., 2016, García-Carnero et al., 2020). Fungal inocula were injected in the last left pro-leg, previously sanitized with 70% (v/v) ethanol, with the assistance of a Hamilton syringe and a 26-gauge needle (Clavijo-Giraldo et al., 2016). The fungal inoculum was of 1×10^5 yeast-like cells 10 μL^{-1}. Larvae were kept in Petri dishes at 37 °C and survival monitored daily for 15 days. To maintain animal hydration, chopped apple was included in the animal housing during the observation period (García-Carnero et al., 2020). The animal silk was removed when evident to delay the transition to the pupa. Loss of irritability and extensive body melanization were taken as signs of insect death. Larvae were analyzed in groups that included 30 animals per experimental condition. As a control, one animal group was injected only with PBS, to assess animal mortality by animal manipulation or mechanical injuries To calculate the colony-forming units (CFUs), alive and dead animals were decapitated with a sterile scalpel, the hemolymph collected, serially diluted, and incubated on YPD plates, pH 4.5, at 28 °C for 72 h.

Hemocytes were quantified in anticoagulated hemolymph as previously reported (García-Carnero et al., 2020); whilst cytotoxicity and phenoloxidase activities were measured in cell-free hemolymph using 20 mM 3,4-dihydroxyDL-phenylalanine (Sigma-Aldrich) and the Pierce LDH Cytotoxicity Assay (Thermo Fisher Scientific), respectively (Martínez-Álvarez et al., 2019, Gómez-Gaviria et al., 2020).

2.12. Statistical analysis

Statistical analysis was performed using GraphPad Prism 6 software. The Mann-Whitney *U* test was used to analyze cytokine stimulation and phagocytosis by human cells. These experiments were carried out in duplicate with samples from eight healthy donors. Animal survival experiments were performed in groups, each containing 30 larvae. Data were analyzed using the Log-rank test and are reported in Kaplan-Meier

survival curves. Other experiments were performed at least three times in duplicate and the unpaired *t*-test was used to establish statistical significance. All data are represented as the mean and standard deviation. In all cases, the significance level was set at $P < 0.05$.

3. Results

3.1. Identification of the S. schenckii RmlD and functional complementation in bacteria

To disrupt the synthesis of rhamnose-containing molecules in *S. schenckii*, we first predicted the putative genes involved in L-rhamnose biosynthesis, using the genome sequence already reported for this organism and the biosynthetic pathway described in *Streptococcus suis* (Martinez et al., 2012, Teixeira et al., 2014). Our analysis indicated that the sequence SPSK_06220 (accession code to GenBank) from *S. schenckii* showed 55% similarity to dTDP-glucose 4,6-dehydratase encoded by *rmlB* (accession code WP_024531966), while SPSK_06451 showed a 48% similarity to dTDP-4-dehydrorhamnose reductase encoded by *rmlD* (WP_174845793). No putative homolog was found for the dTDP-4-dehydrorhamnose 3,5-epimerase encoded for *rmlC*. In *M. grisea,* this biosynthetic pathway has also been described, but differently from prokaryotes, this pathway only involves two enzymes, UG4,6-Dh and U4k6dG-ER, which have UDP-glucose 4,6-dehydratase and UDP-4-dehydrorhamnose 3,5-epimerase/UDP-4-dehydrorhamnose reductase activities, respectively. UG4,6-Dh represents the functional ortholog of RmlB and U4k6dG-ER combines the activity of RmlC and RmlD (Martinez et al., 2012). This bifunctional activity of epimerase and reductase for UG4,6-Dh has also been described for *Botrytis cinerea* bcer and *Botryotinia fuckeliana* U4k6dG-ER (Martinez et al., 2012, Ma et al., 2017). The *S. schenckii* putative proteins encoded by SPSK_06220 and SPSK_06451 showed a similarity of 92% and 91% to UG4,6-Dh and U4k6dG-ER, respectively. *SPSK_06220* and *SPSK_0645* were named here as *RmlB* and *RmlD*, respectively, and were found overexpressed in the yeast morphology, according to the recent transcriptomic analysis of *S. schenckii* dimorphism (Giosa et al., 2020), showing log2FC values of 1.12 and 2.98, respectively. Since the protein encoded by *RmlD* is expected to have a bifunctional role as both epimerase and reductase and the gene showed increased overexpression when compared to *RmlB*, we focused our work on this gene. Bioinformatic analyses showed that RmlD contains a Wierenga motif [10]GASGLLGRQ[18], an Mg^{+2} binding site [137]YGESK[141,] and a catalytic triad [112]T-[137]Y-[141]K found in other RmlD homologs (Blankenfeldt et al., 2002). Moreover, it contains a NAD(P)H binding domain, characteristic of the dehydrogenase/reductase superfamily (Blankenfeldt et al., 2002).

To get insights on the role of RmlD in the biosynthetic pathway of L-rhamnose in *S. schenckii*, heterologous expression and complementation in an *S. mutans* Δ*rmlD* mutant strain were performed (van der Beek et al., 2015). It was previously reported that reduction in the rhamnose content significantly attenuated *S. mutans* growth and affected cell morphology, generating swollen cells and aggregated chains (van der Beek et al., 2015). Heterologous expression with *S. schenckii RmlD*, under the control of a constitutive promoter, restored the *S. mutans* Δ*rmlD* cell morphology in the majority of cells, which formed short chains and grew up unidirectionally. A minority of cells retained the mutant phenotype, i.e., were swollen and aggregated cells (Fig. 2). The growth rate of *S. mutans* Δ*rmlD* expressing *S. schenckii RmlD* was slightly slower than the parental strain, and the buoyancy of *S. mutans* Δ*rmlD* + pSs*RmlD* did not resemble the parental strain, as the cells remained at the bottom of the culture while the WT strain remains in suspension (data not shown). Therefore, these results suggested that *S. schenckii RmlD* partially complemented the truncated biosynthetic pathway found in *S. mutans* Δ*rmlD*.
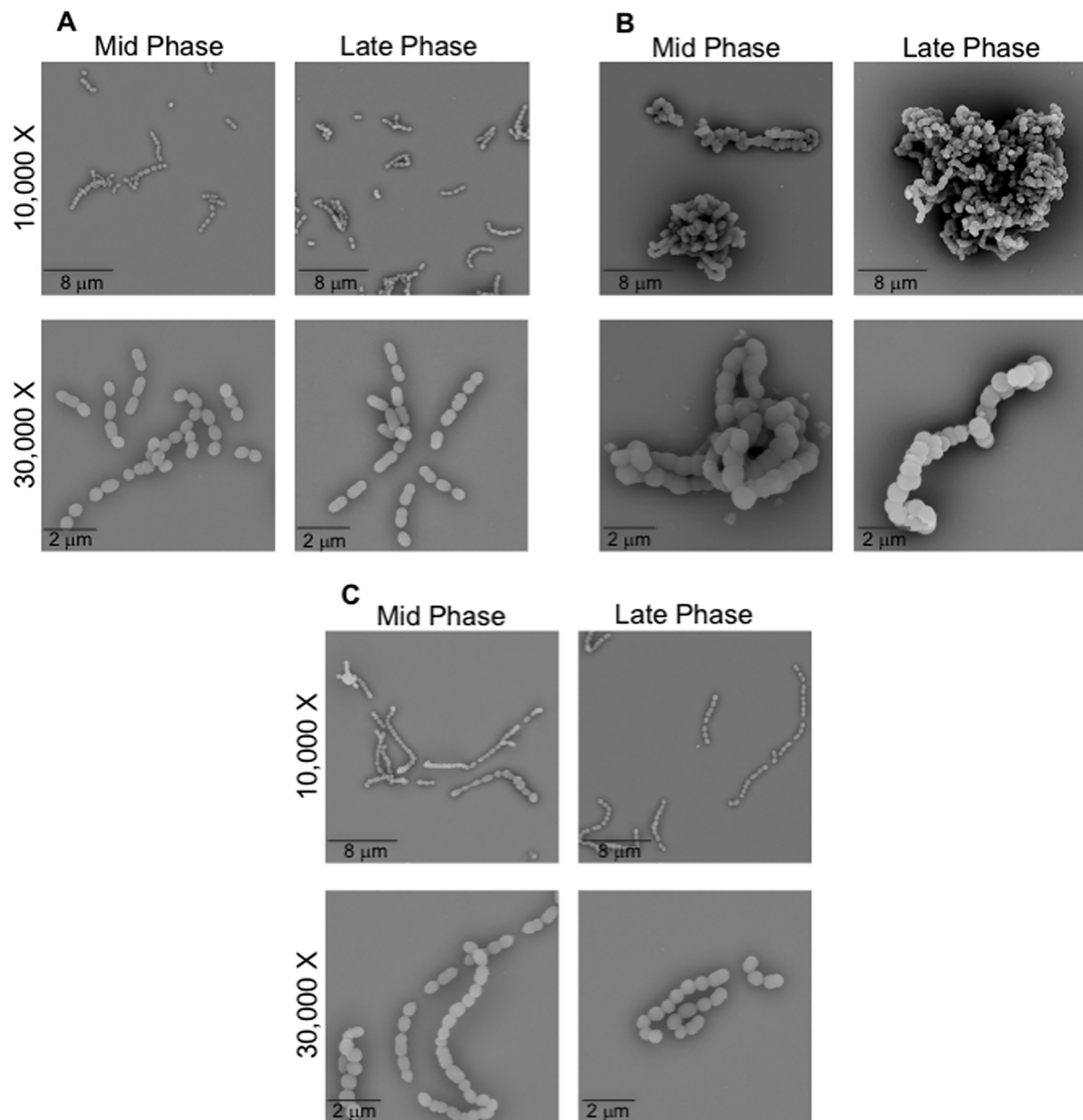
Fig. 2. *Sporothrix schenckii RmlD* partly complements a *Streptococcus mutans* Δ*rmlD* mutant strain. Representative scanning electron microscopy images of *S. mutans* wild type (A), *S. mutans* Δ*rmlD* (B), and *S. mutans* Δ*rmlD* + pSs*RmlD* (C) at different growth times. The cell morphology of the wild-type strain appears as short chains with unidirectional growth, the Δ*rmlD* mutant forms aggregates and long chains with swollen cells. The expression of *S. schenckii RmlD* restored cell morphology, the cells appear as short chains with unidirectional growth, only a few cells are swollen and forming aggregates.

3.2. Sporothrix schenckii RmlD silencing

To assess the *RmlD* relevance in *S. schenckii* fitness and interaction with the host, we generated silenced strains using the previously standardized *A. tumefaciens* mediated-transformation strategy (Lozoya-Pérez et al., 2018, Lozoya-Perez et al., 2019) and the binary vector pBGgHg-*RmlD* constructed here, which contains the first 315 bp of the *RmlD* open reading frame and was cloned in sense and antisense orientations in pBGgHg (Chen et al., 2000). Hygromycin B-resistant cells were selected after transformation, subjected to monoconidial passages, as described in the Materials and methods section, and the insertion of pBGgHg-*RmlD* within the fungal genome was confirmed by PCR (data not shown). Following this strategy, we selected six colonies for further characterization (HSS20-HSS25). *S. schenckii* cells were also transformed with the empty pBGgHg vector and two colonies (HSS29 and

HSS30) were selected and used as controls to assess any specific effects of the vector on the fungal phenotypes.

Changes in *RmlD* expression in the selected mutants were evaluated by RT-qPCR assays, using the gene encoding for the ribosomal protein L6 for data normalization (Trujillo-Esquivel et al., 2017), and the parental strain 1099–18 ATCC MYA 4821, referred here as wild-type (WT), as a reference strain. Both strains HSS29 and HSS30 showed *RmlD* expression levels similar to that observed in the WT strain, confirming that the empty vector did not affect the expression of the target gene (Fig. 3A). However, strains HSS20-HSS25 could be classified into two groups, depending on the *RmlD* silencing degree. HSS20, HSS21, and HSS22 showed a gene silencing of $52.9 \pm 6.9\%$, $50.1 \pm 4.1\%$, and $55.4 \pm 5.6\%$, respectively, while the second group, composed of HSS23, HSS24, and HSS25 showed a gene silencing higher than 98% ($99.7 \pm 1.1\%$, $97.6 \pm 1.2\%$, and $98.5 \pm 0.9\%$, for HSS23, HSS24, and HSS25, respectively;
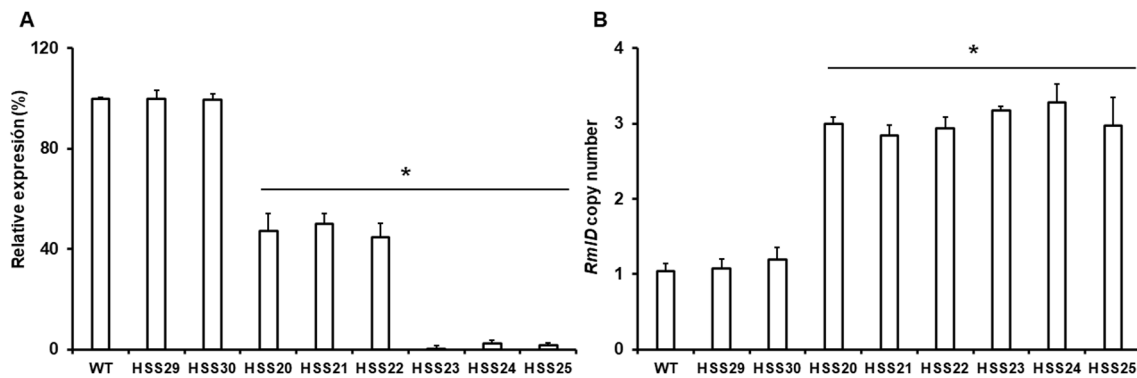
Fig. 3. Analysis of *RmlD* expression and binary vector insertional events. In A, RT-qPCR reactions amplifying a 243 bp fragment of *RmlD* open reading frame were used to assess gene expression. In B, analysis of the binary vector insertional events by qPCR, amplifying the same fragment described in A. In both cases, the amplification of the gene encoding for the ribosomal protein L6 data was used for data normalization. Data are means ± SD of three independent experiments performed in duplicates. *$P < 0.05$ when compared to the WT strain. WT, strain 1099–18 ATCC MYA 4821. Strains HSS29 and HSS30 were transformed with pBGgHg; while HSS20-HSS25 with pBGgHg-*RmlD*.

Fig. 3A). The number of insertional events of the binary plasmid was also evaluated in these selected mutant strains by qPCR, amplifying a 243 bp fragment of the *RmlD* open reading frame. From all the silenced mutants, i.e., HSS20-HSS25 three copies of this *RmlD* fragment were amplified, while from WT and the control strains HSS29 and HSS30 only one *RmlD* amplicon was observed (Fig. 3B). The amplified region is part of the sequence cloned in sense and antisense to generate pBGgHg-*RmlD*, thus the amplification of three copies in the silenced strains can be interpreted as the presence of only one copy of the binary vector per strain and that this occurred in an insertional event outside the *RmlD* locus. Thus, we continued with the phenotypical characterization of the six silenced strains, to assess any potential contribution of the off-target insertional event on the phenotype, along with the strains transformed with the empty vector. When compared to the WT strain, both control and silenced strains showed the same ability to undergo dimorphism, and similar cell and colony morphology (data not shown). Additionally, no apparent growth defect was detected in these strains, as the doubling times for both mycelia and yeast-like cells of the silenced mutants and control strains were similar to those observed in the WT strain (Fig. 4). Therefore, *RmlD* silencing did not affect fungal growth or morphology.

3.3. Cell wall composition and protein glycosylation in the silenced Sporothrix schenckii mutants

Since *RmlD* is likely to participate in the synthesis of nucleotide-activated rhamnose, which is used for protein glycosylation (Ma et al.,

2017), and this monosaccharide is found as part of the *Sporothrix* cell wall (Lopes-Bezerra, 2011, Martinez-Alvarez et al., 2017, Lopes-Bezerra et al., 2018b), we next analyzed the effect of *RmlD* silencing on the *S. schenckii* cell wall composition by HPAEC-PAD. Walls from yeast-like cells were isolated, cleansed, and acid hydrolyzed, before the chromatographic separation of monosaccharides (Mora-Montes et al., 2007, Martinez-Alvarez et al., 2017). Both control strains, HSS29 and HSS30 showed a similar sugar composition to the one observed in the WT strain (Table 2). Since these monosaccharides are the building blocks for chitin (glucosamine), glucans (glucose), and protein-modifying glycans

Table 2
Cell wall analysis of *Sporothrix schenckii* wild-type, control, and *RmlD*-

Cell wall abundance				
Organism	Glucosamine (%)	Mannose (%)	Glucose (%)	Rhamnose (%)
Wild type	4.3 ± 2.5	38.3 ± 3.7	42.2 ± 3.0	15.2 ± 1.7
HSS29	4.5 ± 1.8	39.4 ± 5.4	41.4 ± 5.4	14.7 ± 2.1
HSS30	4.0 ± 1.9	40.5 ± 2.5	39.1 ± 4.4	16.4 ± 2.2
HSS20	5.2 ± 2.6	35.8 ± 3.7	52.4 ± 2.3*	6.6 ± 3.8*
HSS21	5.1 ± 2.2	36.1 ± 4.7	53.1 ± 4.9*	5.7 ± 2.9*
HSS22	5.5 ± 3.4	37.1 ± 2.2	51.7 ± 3.3*	5.7 ± 3.4*
HSS23	4.9 ± 2.0	39.4 ± 2.2	55.0 ± 5.4*	0.7 ± 0.2*
HSS24	5.1 ± 2.4	38.8 ± 3.5	55.9 ± 4.8*	0.2 ± 0.1*
HSS25	4.8 ± 3.1	36.5 ± 4.2	58.4 ± 4.9*	0.3 ± 0.2*

silenced strains
* $P < 0.05$ when compared with the values obtained with the WT strain
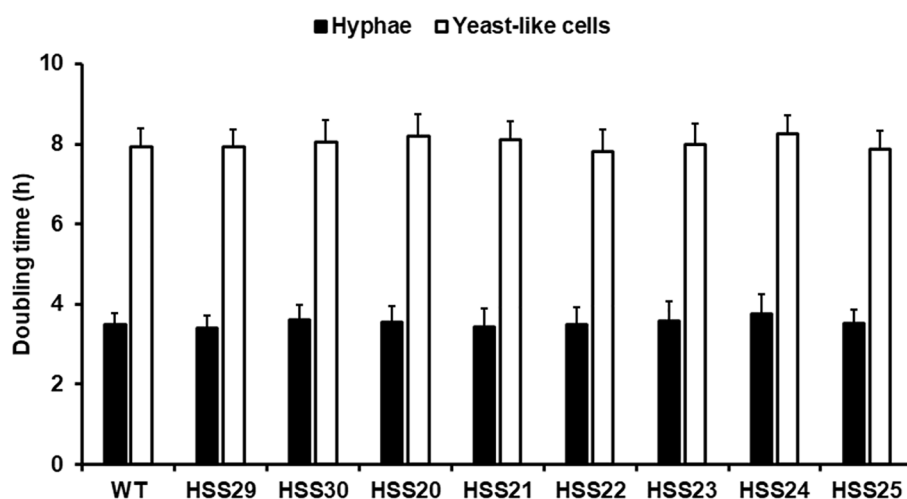
Fig. 4. Doubling times of *Sporothrix schenckii* wild-type, control, and *RmlD*-silenced strains. For hyphae, cells were grown in YPD, pH 4.5, and the biomass dry weight determined every 2 h. For yeast-like cells, these were grown in YPD, pH 7.8, and cells quantified in a hemocytometer. From the generated growth curves, the doubling time was calculated for each strain. WT, strain 1099–18 ATCC MYA 4821. Strains HSS29 and HSS30 were transformed with pBGgHg; while HSS20-HSS25 with pBGgHg-*RmlD*.

(mannose and rhamnose), it is possible to infer the levels of these polysaccharides in the cell walls under analysis (Mora-Montes et al., 2007, Martinez-Alvarez et al., 2017, Lopes-Bezerra et al., 2018b). The strains with intermediate *RmlD* silencing, HSS20-HSS22, showed no differences when compared among them, but there was a significant increment in glucose content and a reduction of about 60% in the rhamnose levels (Table 2). For the rest of the silencing strains, HSS23-HSS25, that showed gene silencing values close to 100%, the cell wall monosaccharide content was similar among the different clones. However, when compared to the WT strain, there was an increment in glucose content and a reduction in rhamnose levels (Table 2). The changes in glucose levels were not significantly different when compared with the mutant group with intermediate silencing, but rhamnose levels were significantly reduced in strains HSS23-HSSS25 with only 2.5% of the total rhamnose content remaining compared to the WT control strain (Table 2). Glucosamine and mannose levels in all the silenced strains were unaffected by *RmlD* silencing (Table 2). We also analyzed cell wall porosity to polycations and the total cell wall protein content and found no significant changes in both parameters in any of the silenced mutant or control strains (80.8 ± 13.4% vs. 76.7 ± 11.7% porosity to DEAE-dextran, WT vs average values of silenced and control strains, respectively, $P = 0.76$; 197.5 ± 23.4 µg of protein mg of cell wall^{-1} vs. 205.4 ± 19.7 µg of protein mg of cell wall^{-1}, WT vs average values of silenced and control strains, respectively, $P = 0.81$). The cell wall ability to bind the cationic dye Alcian blue was also assessed. Although there was a trend to bind more dye by the silenced strains, this was not statistically significant (93.7 ± 12.7, 99.5 ± 13.4, and 115.6 ± 15.7 µg dye bound OD^{600nm} = 1.0^{-1} for the WT, average values of control strains, and average values of silenced strains, respectively, $P = 0.24$).

Since the reduction in rhamnose content suggested a disruption in the proper protein glycosylation pathway, we next enzymatically removed *N*-linked glycans by incubating cells with endoglycosidase H followed by acid hydrolysis of isolated glycans to analyze the monosaccharide content HPAEC-PAD. Results showed that all samples yielded similar amounts of total carbohydrate, and those from the WT and the two control strains contained the same proportion of mannose and rhamnose composing the *N*-linked glycans (Fig. 5A). For strains HSS20-HSS22, there was a significant reduction in rhamnose content of 60% on average, whereas *N*-linked glycans from strains HSS23-HSS25 contained traces amounts of this monosaccharide (Fig. 5A). Even though the mannose content did not change in any of the samples from the silenced mutants, the ratio mannose:total sugar content varied from 0.7 ± 0.04 for WT or control strains to 0.85 ± 0.03 and 0.95 ± 0.01 for strains HSS20-HSS22 and HSS23-HSS25, respectively. In all cases, trace amounts of glucosamine were detected with no significant changes among the different strains analyzed (Fig. 5A). A similar analysis was carried out with *O*-linked glycans trimmed from the cell wall by

β-elimination. WT or control strains contained similar total sugar content and mannose:rhamnose proportion (Fig. 5B). However, for the HSS20-HSS22 intermediate silenced strains a reduction in total sugar and rhamnose was observed, which was even more pronounced in highly silenced strains HSS23-HSS25 (Fig. 5B). Mannose levels did not show significant changes in samples from the silenced strains (Fig. 5B). Collectively, these data indicated that rhamnose bound to both *N*-linked and *O*-linked glycan was reduced in the cell wall of the *RmlD*-silenced strains, and as consequence, cell wall proteins were decorated with mannose-enriched glycans.

Finally, we analyzed whether *RmlD* silencing disrupted the organization of the wall structural polysaccharides chitin and β-1,3-glucan. We focused on both polysaccharides because they are localized closer to the plasma membrane (Martinez-Alvarez et al., 2017, Lopes-Bezerra et al., 2018b). Consequently, detection of large proportions of these polysaccharides at the cell surface is indicative of disruption of the *S. schenckii* cell wall organization (Lozoya-Perez et al., 2019). Polysaccharides were labeled with bulky lectins that are not capable of passing through the cell wall network to bind their targets (Mora-Montes et al., 2011, Marakalala et al., 2013). Therefore, labeling is only observed in areas of the cell wall where these polysaccharides are accessible (Mora-Montes et al., 2011, Martinez-Alvarez et al., 2017, Lozoya-Perez et al., 2019). We included heat-killed (HK) cells as a positive control, since cell inactivation by heat artifactually exposes inner wall components on the cell surface (Gow et al., 2007, Martinez-Alvarez et al., 2017), Results displayed in Fig. 6A indicated that chitin labeling was similar in all analyzed strains, depending on live or HK status, suggesting chitin distribution is not affected by *RmlD* silencing. In contrast, β-1,3-glucan labeling was low and similar in live cells from WT and control strains but was significantly higher in all the *RmlD* silenced strains (HSS20-HSS25; Fig. 6B). As expected, heat inactivation exposed β-1,3-glucan, increasing the labeling in WT and control strains (Fig. 6B). HK cells from all *RmlD* silenced strains showed similar labeling levels that were higher than those observed in WT cells, confirming our earlier observation of higher glucan content in the silenced strains cell wall. Thus, these data indicated that β-1,3-glucan but no chitin is more exposed on the cell surface of strains with *RmlD* silenced.

3.4. The Sporothrix schenckii RmlD silencing affected the cytokine stimulation by human peripheral blood mononuclear cells

We have previously demonstrated that defects in the cell wall composition and protein glycosylation pathways affect the *S. schenckii* ability to stimulate cytokine production by human PBMCs (Lozoya-Perez et al., 2019). Since *RmlD* silencing affected both the cell wall and protein glycosylation, we next analyzed the outcome of the interaction between these mutant cells with human PBMCs, measuring the
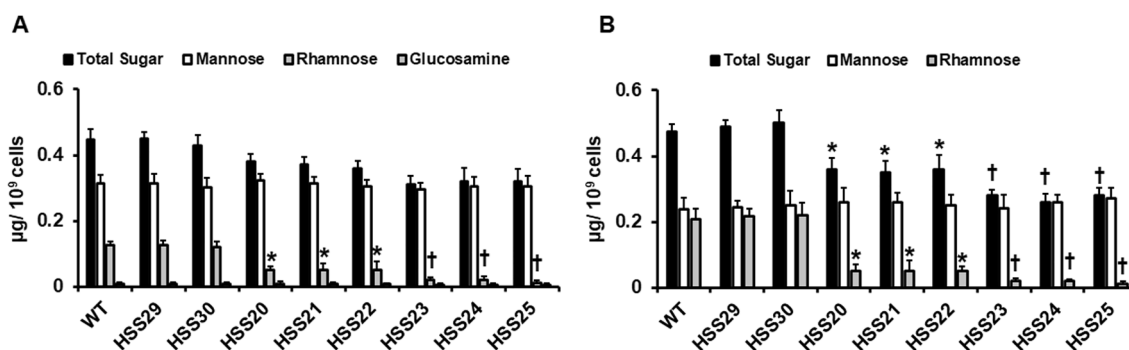
Fig. 5. The *RmlD* silencing in *Sporothrix schenckii* affects the rhamnose content in both *N*-linked and *O*-linked glycans from the cell wall. The *N*-linked (A) or *O*-linked (B) glycans, were trimmed from the cell wall by incubating yeast-like cells with either endoglycosidase H or sodium hydroxide, respectively, the oligosaccharides acid hydrolyzed and monosaccharide content analyzed by High-Performance Anion-Exchange Chromatography with Pulsed Amperometric Detection. Data are means ± SD of three independent experiments performed in duplicates. *$P < 0.05$ when compared to WT or control cells. $^{\dagger}P < 0.05$ when compared to WT or control cells, or HSS20-HSS22 strains. WT, strain 1099–18 ATCC MYA 4821. Strains HSS29 and HSS30 were transformed with pBGgHg; while HSS20-HSS25 with pBGgHg-*RmlD*.
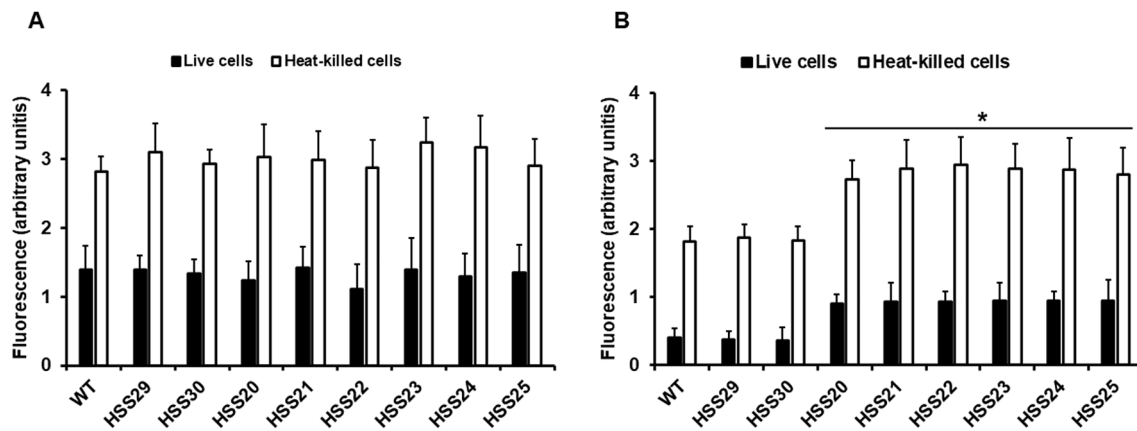
Fig. 6. Cell wall chitin and β-1,3-glucan labeling in *Sporothrix schenckii* wild-type, control, and *RmlD*-silenced strains. Yeast-like cells were labeled with fluorescein isothiocyanate conjugated-wheat germ agglutinin for chitin staining (A) or IgG Fc-Dectin-1 chimera for β-1,3-glucan staining (B) as described in Materials and methods, inspected under fluorescence microscopy, and the fluorescence of 300 cells randomly selected was calculated. Data are means ± SD of three independent experiments performed in duplicates. *$P < 0.05$ when compared to the WT strain. WT, strain 1099–18 ATCC MYA 4821. Strains HSS29 and HSS30 were transformed with pBGgHg; while HSS20-HSS25 with pBGgHg-*RmlD*.

production of soluble TNFα, IL-1β, IL-6, and IL-10. For these four cytokines, the WT and the two control strains, HSS29 and HSS30, stimulated similar cytokine levels (Fig. 7). The strains with intermediate levels of *RmlD* silencing (HSS20, HSS21, and HSS22) induced lower levels of TNFα and IL-6 compared to PBMCs incubated with the WT strain, but this reduction was not significant (P greater than 0.05 in all cases; Fig. 7). In contrast, these three strains stimulated significantly higher levels of both IL-1β and IL-10 (Fig. 7). No differences were observed in the ability to stimulate any of the four cytokines when compared among the three intermediate clones (Fig. 7). Strains HSS23, HSS24, and HSS25, which have nearly abrogated expression of *RmlD*, stimulated similar levels when compared among them, and for the case of TNFα and IL-6, these were significantly lower to those obtained with the WT, the control strains, or HSS20-HSS22 silenced strains (Fig. 7). The IL-1β and IL-10 stimulation by any of these three silenced strains was higher than that obtained with WT cells but similar when compared to strains HSS20-HSS22 (Fig. 7). Therefore, the *RmlD* silencing affected the *S. schenckii* ability to stimulate cytokine production by human PBMCs.
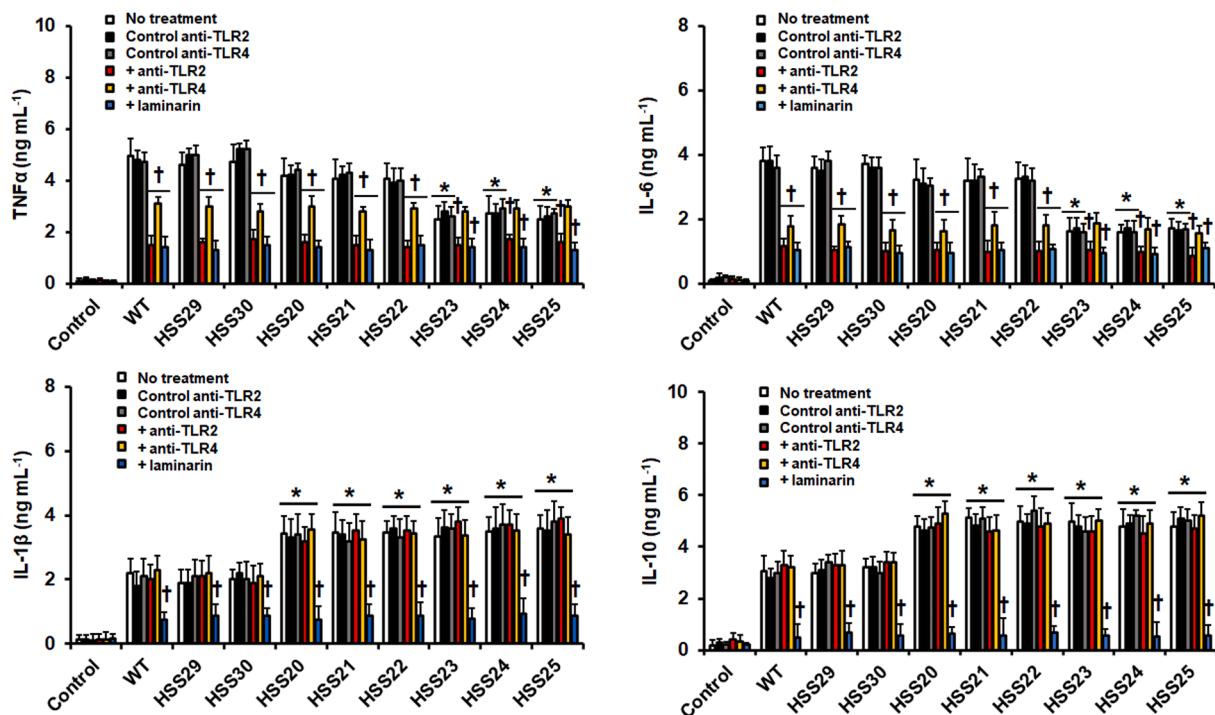
Fig. 7. Cytokine stimulation by human peripheral blood mononuclear cells. Yeast-like cells and human peripheral blood mononuclear cells (PBMCs) were coincubated, the supernatants were collected and the concentration of TNFα, IL-6, IL1β, and IL-10 was measured by ELISA. Data are means ± SD obtained with samples from eight donors, each assayed in duplicate wells. *$P < 0.05$ when compared to WT cells. †$P < 0.05$ when compared to cells under no treatment from the same strain. No treatment, PBMCs preincubated with 5 µg mL^{-1} polymyxin B; Control anti-TLR2, PBMCs preincubated with 5 µg mL^{-1} polymyxin B and 10 µg mL^{-1} IgG$_{2}$aκ; Control anti-TLR4, PBMCs preincubated with 5 µg mL^{-1} polymyxin B and 10 µg mL^{-1} IgG$_{1}$; + anti-TLR2, PBMCs preincubated with 5 µg mL^{-1} polymyxin B and 10 µg mL^{-1} anti-TLR2; + anti-TLR4, preincubated with 5 µg mL^{-1} polymyxin B and 10 µg mL^{-1} anti-TLR4; + laminarin, preincubated with 5 µg mL^{-1} polymyxin B and 200 µg mL^{-1} laminarin. Control, mock reactions were no fungal cells were included. WT, strain 1099–18 ATCC MYA 4821. Strains HSS29 and HSS30 were transformed with pBGgHg; while HSS20-HSS25 with pBGgHg-*RmlD*.

We next assessed the contribution of some immune receptors during the *Sporothrix*-PMBC interaction, by blocking with specific antagonists. We particularly focused on TLR2, TLR4, and dectin-1, because these three receptors have been demonstrated to be major players in the *S. schenckii* immune sensing and for the control of experimental sporotrichosis (Sassá et al., 2012, Negrini et al., 2013, Jellmayer et al., 2017, Martinez-Alvarez et al., 2017). PBMCs preincubation with monoclonal antibodies against TLR2 or TLR4 or laminarin, blocking agents for TLR2, TLR4, or dectin-1, respectively, significantly reduced the TNFα stimulation with WT cells, indicating that these three receptors participate in the signaling pathways to stimulate PBMC cytokine production (Fig. 7). A similar trend was observed with the control strains HSS29 or HSS30, and the silenced strains HSS20-HSS22 (Fig. 7). For TNFα stimulation with the silenced strains HSS23-HSS25, there was a TLR2 and dectin-1 participation to a similar extent than in the systems where the WT or any other of the strains was used (Fig. 7). However, preincubation of PBMCs with anti-TLR4 antibodies did not modify TNFα production stimulated by HSS23, HSS24, or HSS25 (Fig. 7). Control interactions with irrelevant isotype-matched antibodies for anti-TLR2 and anti-TLR4 antibodies stimulated similar cytokine levels than PBMCs without any treatment (Fig. 7). A similar trend was observed for IL-6 stimulation, which was blocked by anti-TLR2, anti-TLR4, or laminarin when PBMCs were incubated with WT, HSS29, HSS30, HSS20-HSS22 (Fig. 7), whereas TLR4 blocking did not affect the ability of strains HSS23-HSS25 to stimulate IL-6 production (Fig. 7). IL1β and IL-10 production were completely dependent on Dectin-1 activation, whereas TLR2 and TLR4 activation were dispensable (Fig. 7).

3.5. Phagocytosis of RmlD-silenced Sporothrix schenckii by human monocyte-derived macrophages

Monocyte-derived macrophages were generated from human PBMCs by differentiation with human granulocyte–macrophage colony-stimulating factor, as reported (Pérez-García et al., 2016). The immune cell-yeast-like cell interactions were analyzed by flow cytometry, as this strategy has been reported to be useful to separate cells in the early, intermediate, or late stage of the phagocytic process, depending on the fluorescence signals emitted (Hernández-Chávez et al., 2018, Lozoya-Pérez et al., 2018, Lozoya-Perez et al., 2019). The WT and the

control strains HSS29 and HSS30 showed similar abilities to interact with the human immune cells, and no differences in any of the three defined stages were observed among these strains (Fig. 8A). The silenced strains HSS20-HSS25 showed similar phagocytosis levels and the number of immune cells in the early, intermediate, or late stage of the phagocytic event was significantly higher than those observed in the WT or control strains (Fig. 8A). Mock reactions, where human monocyte-derived cells were analyzed in the absence of *S. schenckii* showed only threshold cell numbers for any of the three defined stages (Fig. 8A). Therefore, the *S. schenckii*-human-derived macrophage interaction was significantly affected by *RmlD* silencing.

To gain insight into the receptors involved in the phagocytic process, we next preincubated the human cells with agents that block specific receptors and assessed the impact on the number of immune cells interacting with fungal cells. We particularly focused on cells in the late stage of the phagocytic process because this provided differences well defined between the WT and silenced strains (Fig. 8A). Results in Fig. 8B showed that preincubation of human monocyte-derived macrophages with anti-TLR2 antibodies decreased the cell number interacting with yeast-like cells by $18.1 \pm 5.7\%$ in all strains analyzed, indicating a minor contribution for this receptor during the phagocytic process and in a similar extent in WT, control, and silenced strains (Fig. 8B). Control reactions with an irrelevant isotype-matched antibody showed no effects on the ability of immune cells to phagocyte fungal cells (data not shown). When similar experiments were conducted with immune cells preincubated with anti-TLR4 antibodies, we found about a $25.5 \pm 5.1\%$ reduction in the phagocytosis of WT or control strains (Fig. 8B). This effect was partially lost when the silenced strains HSS20-HSS22 were interacting with immune cells (reduction of about $15.1 \pm 4.2\%$) and was lost in the systems where HSS23-HSS25 strains were included (Fig. 8B). These data suggested that the blocking effect of anti-TLR4 antibodies was lost in the silenced strains HSS23-HSS25, most likely because the TLR4 ligand was absent, i.e., rhamnose. To confirm this observation, we preincubated the human cells with rhamnose before challenged with the fungal cells. In pilot experiments, we found that the minimal rhamnose concentration to block fungal phagocytosis was 200 μg mL^{-1}, and increased concentrations did not significantly change this effect (data not shown). After preincubation with 200 μg mL^{-1} rhamnose, the monocyte-derived macrophages showed a reduction in the ability to
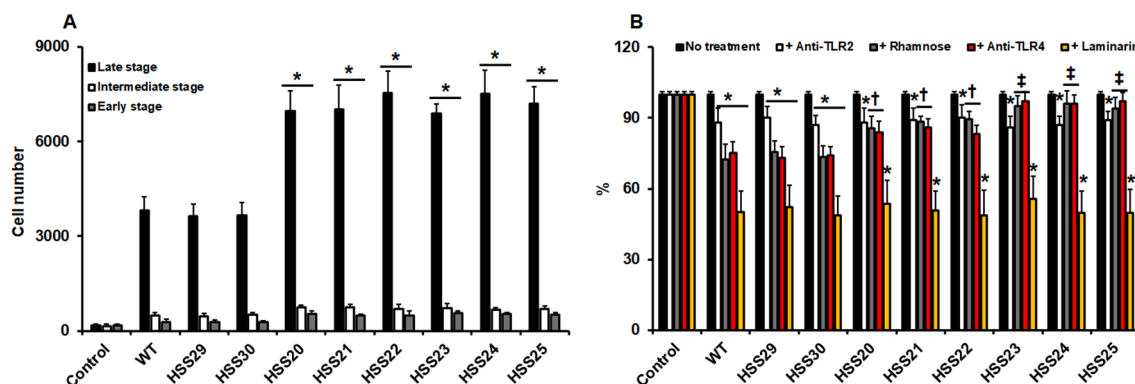
Fig. 8. Phagocytosis of *RmlD*-silenced *S. schenckii* by human monocyte-derived macrophages. In A, Acridine Orange-labeled yeast-like cells were coincubated with human monocyte-derived macrophages at a macrophage-yeast ratio 1:6, for 2 h at 37 °C and 5% (v/v) CO$_2$. The macrophages were gated by FACS and 50,000 cells were counted per sample. Macrophages interacting with at least one fluorescent yeast cell were included as counted events. Control, macrophages interacting with no yeast-like cells. *$P < 0.05$ when compared to WT strain. In B, similar experiments to those described in panel A were performed but with human cells previously preincubated with 5 μg mL^{-1} polymyxin B and 10 μg mL^{-1} anti-TLR2 (+anti-TLR2), with 5 μg mL^{-1} polymyxin B and 200 μg mL^{-1} L-rhamnose (+Rhamnose), 5 μg mL^{-1} polymyxin B and 10 μg mL^{-1} anti-TLR4 (+anti-TLR4), or with 5 μg mL^{-1} polymyxin B and 200 μg mL^{-1} laminarin (+Laminarin). No treatment refers to cells preincubated only with 5 μg mL^{-1} polymyxin B. Results correspond to cells in the late stage of phagocytosis. For all cases, 100% corresponds to the system with no treatment and the absolute values were similar to those shown in panel A. Control, macrophages interacting with no yeast-like cells. *$P < 0.05$ when compared to the no treatment condition of the same strain. † $P < 0.05$ when compared to the no treatment condition of the same strains and other strains under the same condition. ‡ $P < 0.05$ when compared to WT strain under the same condition. For both panels, data represent means $\pm$ SD from six donors assayed by duplicate. WT, strain 1099–18 ATCC MYA 4821. Strains HSS29 and HSS30 were transformed with pBGgHg; while HSS20-HSS25 with pBGgHg-*RmlD*. (For interpretation of the references to colour in this figure legend, the reader is referred to the web version of this article.)

phagocyte the WT or control cells similar to that observed when TLR4 was blocked, and this effect was partially lost in the silenced strains HSS20-HSS22 and absent in the strains HSS23-HSS25 (Fig. 8B). The blocking of dectin-1 by laminarin reduced fungal phagocytosis by about $50.3 \pm 8.9\%$ and this observation was similar for all the strains analyzed (Fig. 8B). Therefore, different receptors contribute to *S. schenckii* yeast-like cells phagocytosis, and TLR4 is required to mediate *S. schenckii* phagocytosis by a rhamnose-dependent mechanism.

3.6. RmlD silencing affected the Sporothrix schenckii virulence in Galleria mellonella larvae

To assess whether the *RmlD* silencing affected the ability of *S. schenckii* to kill the host, we infected *Galleria mellonella* larvae with the different strains used in this study and compared the survival. We selected this alternative model to evaluate virulence because it provides basic lethality parameters of fungal strains similar to that generated with mice (Clavijo-Giraldo et al., 2016, Lozoya-Pérez et al., 2018, Lozoya-Perez et al., 2019, Lozoya-Pérez et al., 2020, Macêdo-Sales et al., 2020). Results showed that groups inoculated with the WT or the control strains HSS29 and HSS30 have similar median survival times of 6.0 ± 0.5 days and killed about $74.5 \pm 5.1\%$ of the insect population after the two-week observation period (Fig. 9). No significant differences were observed among these three fungal strains (Fig. 9). Incubation of *Galleria* with strains HSS20-HSS22 resulted in a median survival time of 12.0 ± 0.2 days killing $40.0 \pm 3.3\%$ of insects (Fig. 9). The mortality curves generated with strains HSS23-HSS25 were similar among them, but in contrast to the rest of the strains under analysis, most of the insect population survived at the end of the observation period, with median survivals of more than 15 days and killing only $3.0 \pm 0.5\%$ of the infected population (Fig. 9). The defect in the ability to kill insects was unlikely to be associated with defects in fungal cells to grow inside larvae, as similar CFUs were recovered from insects inoculated with the WT, control, or silenced strains (Table 3). The *Galleria* control group inoculated only with PBS showed 100% survival during the observation period (data not shown). Next, we analyzed whether this increased survival in insects infected with *RmlD*-silenced strains could be associated with decreased effects on cell damage inside the larva body, measured as the cell-free lactate dehydrogenase found in the hemocele (García-Carnero et al., 2020, Gómez-Gaviria et al., 2020, Lozoya-Pérez et al., 2020), and referred here as cytotoxicity. As expected, high and
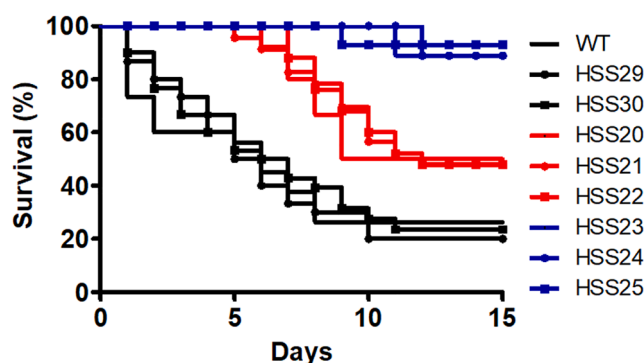
Fig. 9. Mortality of *Galleria mellonella* larvae inoculated with *RmlD*-silenced *Sporothrix schenckii*. Groups containing 30 larvae were inoculated with 1×10^5 yeast-like cells in 10 μL of PBS and survival recorded daily for 15 days. Data are shown in Kaplan–Meier plots. The statistical analysis showed no differences among the WT, HSS29, and HSS30 strains ($P = 0.68$), but the silenced strains generated survival curves with significantly increased median survival times ($P < 0.05$). When compared among them, no differences were observed in the curves generated with strains HSS20, HSS21, and HSS22 ($P = 0.76$), nor with those generated with strains HSS23, HSS24, and HSS25 ($P = 0.88$). WT, strain 1099–18 ATCC MYA 4821. Strains HSS29 and HSS30 were transformed with pBGgHg; while HSS20-HSS25 with pBGgHg-*RmlD*.

Table 3

Fungal burden, cytotoxicity, hemocyte, and phenoloxidase levels in *Galleria mellonella* inoculated with *RmlD*-silenced *Sporothrix schenckii*.

Strain	Colony-Forming Units ($\times 10^5$) [a]	Cytotoxicity (%) [b]	Hemocytes ($\times 10^6$) mL^{-1} [c]	Phenoloxidase [d]
PBS [e]	0.0 ± 0.0	15.5 ± 4.8	3.2 ± 0.5	0.6 ± 0.3
WT [f]	2.5 ± 0.6	81.4 ± 11.4	8.3 ± 0.7	3.0 ± 0.4
HSS29	2.6 ± 0.5	87.5 ± 13.0	7.7 ± 0.8	3.1 ± 0.2
HSS30	2.9 ± 0.7	79.8 ± 9.7	8.1 ± 0.7	3.3 ± 0.4
HSS20	2.6 ± 0.4	56.7 ± 10.5 * †	6.0 ± 0.4 * †	2.2 ± 0.5 * †
HSS21	2.5 ± 0.7	50.4 ± 11.4 * †	5.7 ± 0.3 * †	2.0 ± 0.5 * †
HSS22	2.5 ± 0.6	50.1 ± 10.0 * †	5.6 ± 0.6 * †	2.1 ± 0.3 * †
HSS23	2.8 ± 0.5	28.5 ± 8.8 *	4.2 ± 0.5 *	1.2 ± 0.3 *
HSS24	2.9 ± 0.8	24.1 ± 6.6 *	4.2 ± 0.6 *	1.0 ± 0.3 *
HSS25	2.8 ± 0.9	28.9 ± 11.8 *	4.5 ± 0.4 *	0.9 ± 0.4 *

[a] Surviving and dead animals were decapitated, and the hemolymph from dead and survival animals was collected and used to calculate the colony-forming units by incubating on YPD plates.
[b] Refers to the free lactate dehydrogenase activity quantified in the cell-free hemolymph from inoculated insects. Data were normalized to the enzyme activity determined in lysed hemocytes, which were considered as the 100%.
[c] Calculated from the infected animals' hemolymph.
[d] Calculated in the cell-free hemolymph and defined as the Δ_{490nm} min^{-1} μg protein $^{-1}$.
[e] Control group inoculated only with PBS.
[f] WT, strain 1099–18 ATCC MYA 4821. Strains HSS29 and HSS30 were transformed with pBGgHg; while HSS20-HSS25 with pBGgHg-*RmlD*. * $P < 0.05$ when compared with the values obtained in animals infected with the WT strain.
† $P < 0.05$ when compared with the measurements in animals infected with the WT or HSS23-HSS25 strains.

similar cytotoxicity levels were observed in the insect groups inoculated with the WT or the HSS29 and HSS30 control strains, and this parameter was significantly reduced in the groups inoculated with strains HSS20, HSS21, or HSS22 (Table 3). Interestingly, cytotoxicity in the larvae inoculated with strains HSS23, HSS24, or HSS25 was even lower and significantly different from the levels observed in the other silenced strains, the WT or the control strains (Table 3). The insect immune effectors, hemocytes, and phenol oxidase have been recently reported to be responsive defense elicitors that are modulated depending on the *Sporothrix* virulence (Lozoya-Pérez et al., 2020). Therefore, we quantified these two parameters in the insect groups inoculated with the silences strains.

Results indicated that the highest hemocyte countings and phenoloxidase activity were found in the larvae inoculated with the WT, or the control strains HSS29 or HSS30, whereas groups infected with strains HSS20-HSS22 showed significantly lower levels of both parameters (Table 3). The groups infected with strains HSS23-HSS25 showed similar values of both hemocytes and phenoloxidase activity and these were lower when compared to those generated by the WT, control, or other silenced strains (Table 3). Collectively, these data indicated that *RmlD* silencing negatively affected the *S. schenckii* ability to kill *G. mellonella* larvae and the ability to stimulate insect immune effectors.

4. Discussion

S. schenckii is one of the causative agents of sporotrichosis, an acute or chronic granulomatous subcutaneous mycosis (Mora-Montes et al., 2015). As with other pathogenic fungi, the cell wall modulates the interaction with the host immune system, and contains species-specific components (Netea et al., 2008, Arana et al., 2009, Díaz-Jiménez et al., 2012, Martínez-Álvarez et al., 2014, Martinez-Alvarez et al., 2017, Lopes-Bezerra et al., 2018b, Garcia-Rubio et al., 2020). One of the most distinctive *S. schenckii* cell wall components is the presence of

glycoproteins modified with glycans consisting of mannose and rhamnose, which is a complex of different macromolecules that collectively are named peptidorhamnomannan (Lloyd and Bitoon, 1971, Lopes-Bezerra, 2011, Mora-Montes et al., 2015, Lopes-Bezerra et al., 2018b).

The L-rhamnose biosynthetic pathway has been described in bacteria, plants, and some fungal species (Giraud and Naismith, 2000, Blankenfeldt et al., 2002, Watt et al., 2004, Martinez et al., 2012, Ma et al., 2017, Wagstaff et al., 2019). Our search within the *S. schenckii* genome for putative orthologous genes encoding for enzymes participating in L-rhamnose synthesis identified only two possible candidates, similar to other fungal systems (Ma et al., 2017). Both *RmlB* and *RmlD* are overexpressed in the yeast-like cells (Giosa et al., 2020), correlating with the observations that in this morphology a higher cell wall rhamnose content is found than in hyphae (Martinez-Alvarez et al., 2017). Heterologous complementation in *S. mutants* showed that the *Sporothrix RmlD* gene restored the aberrant growth and morphology phenotype of *S. mutans* Δ*rmlD* almost to a level similar to that observed in the parental strain, strongly suggesting its participation in L-rhamnose synthesis. It is worth mentioning that not all cells within the population showed a restored phenotype. This may be explained because *S. schenckii* RmlD has a slower activity rate than the native enzyme because of its inability to form dimers in the bacterial milieu, which is essential for the activity of many enzymes (Giraud and Naismith, 2000). In addition, enzyme performance could also be affected by the nucleotide bound to the monosaccharide, which differs between bacteria and fungi (Martinez et al., 2012). Indeed, it has been reported that the UDP binding to the nucleotide-diphosphate domain enhances the reactivity of NAD^+ in short-chain dehydrogenase/reductase enzymes, an enzyme family where RmlD is grouped (Kavanagh et al., 2008). Another explanation is that *S. schenckii* RmlD competes with *S. mutans* RmlC for the substrate, leading to a less amount of rhamnose in the cells. Nonetheless, these results, along with the reduction in rhamnose content upon *RmlD* silencing support the notion that this gene participates in the *S. schenckii* rhamnose synthesis.

The molecular tools for the *S. schenckii* genomic manipulation are currently scarce, and thus we included the well-characterized methodology for gene silencing (Rodriguez-Caban et al., 2011, Lozoya-Perez et al., 2019). Even though the insertion of the binary plasmid is random, the inclusion of three independent mutants with similar silencing levels allowed us to discard that the observed phenotypes could be due to insertional events rather than the *RmlD* silencing.

Rhamnose biosynthesis is essential in bacteria such as *Streptococcus pyogenes* and *Mycobacterium smegmatis* (Ma et al., 2002, van der Beek et al., 2015) but dispensable in fungi, having minimal contributions on cell morphology or development (Ma et al., 2017, Santhanam et al., 2017). In agreement with these observations, we found here that *RmlD* silencing, and therefore rhamnose depletion did not affect the doubling time, cell and colony morphology, and ability to undergo dimorphism. It is thought that binding of L-rhamnose to *N*-linked and *O*-linked glycans is a terminal event (Lopes-Bezerra, 2011). This would offer a possible explanation of the lack of a severe phenotype in *RmlD*-silencing mutant cells. In *B. cinerea*, upon disruption of the *RmlD* the accumulation of UDP-4-keto-6-deoxy-glucose, the RmlD substrate, led to defects in cell morphology (Ma et al., 2017). The apparent discrepancy of this observation with our results could be explained by the fact that residual *RmlD* transcription was found in the HSS23-HSS25, and this could avoid the accumulation of toxic levels of this compound. Alternatively, UDP-4-keto-6-deoxy-glucose may indeed accumulate in the *S. schenckii RmlD*-silenced strains and this species simply has a different sensitivity degree to UDP-4-keto-6-deoxy-glucose when compared to that observed in *B. cinerea*.

The cell wall integrity pathway is a signaling network that allows the fungal cell to respond and adapt to stresses that affect the wall, including permanent modifications such as the ones generated by mutations (Bates et al., 2006, Mora-Montes et al., 2007, Valiante, 2017). The increment in β-1,3-glucan content and exposure at the cell surface is likely a consequence of this pathway activation upon reduction of rhamnose content in the silenced mutants. In line with this, *Candida* spp. mutant strains, where mannan elaboration is disrupted, showed increased β-1,3-glucan content as a compensatory mechanism to the weakness of the cell wall outer layer (Bates et al., 2005, Bates et al., 2006, Mora-Montes et al., 2007, Mora-Montes et al., 2010a, Navarro-Arias et al., 2016, Pérez-García et al., 2016, Hernández-Chávez et al., 2019), and interestingly, the disruption of the *N*-linked glycan outer chain elaboration in *S. schenckii* had as a consequence a reduction in rhamnose content and increment in glucan levels (Lozoya-Perez et al., 2019), suggesting that rhamnose levels attached to *N*-linked glycans could be the sensors that trigger activation of the cell wall integrity pathway. A second possible explanation to this observation, which does not exclude the previous one, is that both β−1,3-glucan and rhamnose biosynthetic pathways share UDP-glucose as the same precursor, and therefore, disruption of the rhamnosylation pathway might increase the precursor levels that are used in the synthesis of this wall structural polysaccharide. We currently do not have a feasible explanation for the fact that only one polysaccharide was modified in these cells and this is an observation that remains to be addressed. Despite rhamnose reduction was observed in both *N*-linked and *O*-linked glycans from *RmlD*-silenced strains, this did not significantly change the total sugar content in *N*-linked glycans, suggesting rhamnose is not the main component of these structures, and supporting the notion that it is a monosaccharide that modifies the branches attached to the outer chain (Lopes-Bezerra, 2011, Teixeira et al., 2014, Lopes-Bezerra et al., 2018a). On the contrary, rhamnose reduction led to a significantly minor total sugar content in the *O*-linked glycans from the *RmlD*-silenced strains, suggesting that rhamnose has a significant contribution to their structure, as previously reported for the case of the peptidorhamnomannan *O*-linked glycans (Lopes-Bezerra, 2011). Thus, we hypothesize that *O*-linked glycans in the silenced mutant are shorter than those found in the WT strain, making the cell wall outer layer thinner and less bulky, allowing β-1,3-glucans to be more exposed at the surface

The *RmlD*-silenced mutants showed a differential ability to stimulate cytokine production by human PBMCs, and as consequence lower TNFα and IL-6 levels but higher IL-1 β and IL-10 production were observed when compared to WT cells. The use of blocking agents suggested that TLR4 is the receptor for rhamnose present in the *S. schenckii* cell wall, and this observation is in line with a previous report, which indicates that this immune receptor recognizes *P. boydii* rhamnomannan (Figueiredo et al., 2010). The production of both TNFα and IL-6 by human PBMCs depends mainly on the engagement of dectin-1, TLR2, and TLR4 with their ligands (Martinez-Alvarez et al., 2017), and most likely in a co-stimulatory event (Dennehy et al., 2008, Netea et al., 2008, Reid et al., 2009). Thus, the reduction of the TLR4 ligand in the *RmlD*-silenced mutants could account for the observed changes in the levels of these proinflammatory cytokines. When interacting with *S. schenckii*, dectin-1 is the main PBMCs receptor required for IL-1 β and IL-10 production (Martinez-Alvarez et al., 2017), thus, it is likely that the increased β-1,3-glucan content and exposure at the cell surface positively influenced the ability of the mutant strains to stimulate both IL-1 β and IL-10. Dectin-1 is predominantly expressed in macrophages (Taylor et al., 2002), and its engagement with the ligand is sufficient to trigger phagocytosis (Heinsbroek et al., 2008). Therefore, our finding reported here about the *Sporothrix*-macrophage interaction is likely explained by dectin-1 dependent phagocytosis. However, our observations also indicate that the TLR4-L-rhamnose interplay, and to a lesser extent the TLR2-ligand interaction are also relevant during the sensing of this fungal species by human monocyte-derived macrophages.

The *RmlD*-silenced mutants showed virulence attenuation in the *G. mellonella* infection model, suggesting that rhamnose is required to display the ability to kill larvae. This virulence attenuation is unlikely to *in vivo* growth defect, as similar fungal burdens were found in WT, control, and silenced strains. This observation is in line with those in *B. cinerea* and *Verticillium dahlia*, where rhamnose-depleted mutants lost the

ability to colonize and cause damage to the host (Ma et al., 2017, Santhanam et al., 2017). It is worthy of mention that these are phytopathogens, and our study here with *S. schenckii* reports for the first time a link between virulence and rhamnose in a mammalian's fungal pathogen. The fungal adhesion to host cells is crucial for colonization and dissemination, and in *S. schenckii* exists a correlation between the virulence and the interaction of adhesins with fibronectin (Teixeira et al., 2009). The loss of rhamnose from the *S. schenckii* cell wall could affect the cell's ability to adhere properly to the host cells, as both the peptidorhamnomannan and rhamnose have been described as part of the adhesive mechanism molecules (Pinto et al., 2004, Santhanam et al., 2017), possibly explaining the virulence attenuation upon *RmlD* silencing.

In conclusion, *S. schenckii RmlD* is involved in the synthesis of L-rhamnose and the presence of this carbohydrate at the cell wall is important during the interaction of this fungus with human PBMCs and monocyte-derived macrophages, in TLR4-dependent mechanisms. Moreover, *RmlD* is required for *S. schenckii* virulence.

CRediT authorship contribution statement

Alma K. Tamez-Castrellón: Data curation, Formal analysis, Writing - original draft. **Samantha L. van der Beek:** Data curation, Formal analysis, Writing - original draft, Writing - review & editing, Writing - review & editing. **Luz A. López-Ramírez:** Data curation, Formal analysis, Project administration, Writing - original draft, Writing - review & editing. **Iván Martínez-Duncker:** Data curation, Formal analysis, Writing - original draft, Writing - review & editing. **Nancy E. Lozoya-Pérez:** Data curation, Formal analysis, Writing - original draft, Writing - review & editing. **Nina M. van Sorge:** Data curation, Formal analysis, Funding acquisition, Writing - original draft, Writing - review & editing. **Héctor M. Mora-Montes:** Data curation, Formal analysis, Funding acquisition, Project administration, Writing - original draft, Writing - review & editing.

Declaration of Competing Interest

The authors declare that they have no known competing financial interests or personal relationships that could have appeared to influence the work reported in this paper.

References

Arana, D.M., Prieto, D., Román, E., Nombela, C., Alonso-Monge, R., Pla, J., 2009. The role of the cell wall in fungal pathogenesis. Microb Biotechnol 2 (3), 308–320.

Bates, S., Hughes, H.B., Munro, C.A., Thomas, W.P.H., MacCallum, D.M., Bertram, G., Atrih, A., Ferguson, M.A.J., Brown, A.J.P., Odds, F.C., Gow, N.A.R., 2006. Outer chain *N*-glycans are required for cell wall integrity and virulence of *Candida albicans*. J Biol Chem 281 (1), 90–98.

Bates, S., MacCallum, D.M., Bertram, G., Munro, C.A., Hughes, H.B., Buurman, E.T., Brown, A.J.P., Odds, F.C., Gow, N.A.R., 2005. *Candida albicans* Pmr1p, a secretory pathway P-type Ca^{2+}/Mn^{2+}-ATPase, is required for glycosylation and virulence. J Biol Chem 280 (24), 23408–23415.

Blankenfeldt, W., Kerr, I.D., Giraud, M.-F., McMiken, H.J., Leonard, G., Whitfield, C., Messner, P., Graninger, M., Naismith, J.H., 2002. Variation on a theme of SDR: dTDP-6-deoxy-L- lyxo-4-hexulose reductase (RmlD) shows a new Mg^{2+}-dependent dimerization mode. Structure 10 (6), 773–786.

Castro, R.A., Kubitschek-Barreira, P.H., Teixeira, P.A.C., Sanches, G.F., Teixeira, M.M., Quintella, L.P., Almeida, S.R., Costa, R.O., Camargo, Z.P., Felipe, M.S.S., de Souza, W., Lopes-Bezerra, L.M., Wormley, Jr., F., 2013. Differences in cell

morphometry, cell wall topography and Gp70 expression correlate with the virulence of *Sporothrix brasiliensis* clinical isolates. PLoS ONE 8 (10), e75656.

Chaffin, D.O., Rubens, C.E., 1998. Blue/white screening of recombinant plasmids in Gram-positive bacteria by interruption of alkaline phosphatase gene (phoZ) expression. Gene 219 (1-2), 91–99.

Chakrabarti, A., Bonifaz, A., Gutierrez-Galhardo, M.C., Mochizuki, T., Li, S., 2015. Global epidemiology of sporotrichosis. Med Mycol 53 (1), 3–14.

Chen, X.i., Stone, M., Schlagnhaufer, C., Romaine, C.P., 2000. A fruiting body tissue method for efficient *Agrobacterium*-mediated transformation of *Agaricus bisporus*. Appl Environ Microbiol 66 (10), 4510–4513.

Clavijo-Giraldo, D.M., Matínez-Alvarez, J.A., Lopes-Bezerra, L.M., Ponce-Noyola, P., Franco, B., Almeida, R.S., Mora-Montes, H.M., 2016. Analysis of *Sporothrix schenckii sensu stricto* and *Sporothrix brasiliensis* virulence in *Galleria mellonella*. J Microbiol Methods 122, 73–77.

de Beer, Z.W., Duong, T.A., Wingfield, M.J., 2016. The divorce of *Sporothrix* and *Ophiostoma*: solution to a problematic relationship. Stud Mycol 83, 165–191.

De Nobel, J.G., Klis, F.M., Munnik, T., Priem, J., Van Den Ende, H., 1990. An assay of relative cell wall porosity in *Saccharomyces cerevisiae*, *Kluyveromyces lactis* and *Schizosaccharomyces pombe*. Yeast 6 (6), 483–490.

Dennehy, K.M., Ferwerda, G., Faro-Trindade, I., Pyż, E., Willment, J.A., Taylor, P.R., Kerrigan, A., Tsoni, S.V., Gordon, S., Meyer-Wentrup, F., Adema, G.J., Kullberg, B.-J., Schweighoffer, E., Tybulewicz, V., Mora-Montes, H.M., Gow, N.A.R., Williams, D.L., Netea, M.G., Brown, G.D., 2008. Syk kinase is required for collaborative cytokine production induced through Dectin-1 and Toll-like receptors. Eur J Immunol 38 (2), 500–506.

Díaz-Jiménez, D.F., Pérez-García, L.A., Martínez-Álvarez, J.A., Mora-Montes, H.M., 2012. Role of the fungal cell wall in pathogenesis and antifungal resistance. Curr Fungal Infect Rep 6 (4), 275–282.

DuBois, M., Gilles, K.A., Hamilton, J.K., Rebers, P.A., Smith, F., 1956. Colorimetric method for determination of sugars and related substances. Anal Chem 28 (3), 350–356.

Endres, S., Ghorbani, R., Lonnemann, G., van der Meer, J.W., Dinarello, C.A., 1988. Measurement of immunoreactive interleukin-1 beta from human mononuclear cells: optimization of recovery, intrasubject consistency, and comparison with interleukin-1 alpha and tumor necrosis factor. Clin Immunol Immunopathol 49, 424–438.

Estrada-Mata, E., Navarro-Arias, M.J., Perez-Garcia, L.A., Mellado-Mojica, E., Lopez, M.G., Csonka, K., et al., 2015. Members of the *Candida parapsilosis* complex and *Candida albicans* are differentially recognized by human peripheral blood mononuclear cells. Front Microbiol 6, 1527.

Figueiredo, R.T., Fernandez, P.L., Dutra, F.F., González, Y., Lopes, L.C., Bittencourt, V.C.B., Sassaki, G.L., Barreto-Bergter, E., Bozza, M.T., 2010. TLR4 recognizes *Pseudallescheria boydii* conidia and purified rhamnomannans. J Biol Chem 285 (52), 40714–40723.

García-Carnero, L.C., Clavijo-Giraldo, D.M., Gómez-Gaviria, M., Lozoya-Pérez, N.E., Tamez-Castrellón, A.K., López-Ramírez, L.A., Mora-Montes, H.M., 2020. Early virulence predictors during the *Candida* species-*Galleria mellonella* interaction. J Fungi (Basel) 6 (3), 152. https://doi.org/10.3390/jof6030152.

R. Garcia-Rubio H.C. de Oliveira J. Rivera N. Trevijano-Contador The fungal cell wall: Candida, Cryptococcus, and Aspergillus species. Front Microbiol 10 10.3389/fmicb.2019.02993.

Garufi, G., Hendrickx, A.P., Beeri, K., Kern, J.W., Sharma, A., Richter, S.G., Schneewind, O., Missiakas, D., 2012. Synthesis of lipoteichoic acids in *Bacillus anthracis*. J. Bacteriol. 194 (16), 4312–4321.

D. Giosa M.R. Felice L. Giuffrè R. Aiese Cigliano A. Paytuví-Gallart C. Lo Passo C. Barresi E. D'Alessandro H. Huang G. Criseo H.M. Mora-Montes S. de Hoog O. Romeo Transcriptome-wide expression profiling of Sporothrix schenckii yeast and mycelial forms and the establishment of the Sporothrix Genome DataBase 6 10 2020 10.1099/mgen.0.000445.

Giraud, M.-F., Naismith, J.H., 2000. The rhamnose pathway. Curr Opin Struct Biol 10 (6), 687–696.

Gómez-Gaviria, M., Lozoya-Pérez, N.E., Staniszewska, M., Franco, B., Niño-Vega, G.A., Mora-Montes, H.M., 2020. Loss of Kex2 affects the *Candida albicans* cell wall and interaction with innate immune cells. J Fungi (Basel) 6 (2), 57. https://doi.org/10.3390/jof6020057.

González-Hernández, R.J., Jin, K., Hernández-Chávez, M.J., Díaz-Jiménez, D.F., Trujillo-Esquivel, E., Clavijo-Giraldo, D.M., Tamez-Castrellón, A.K., Franco, B., Gow, N.A.R., Mora-Montes, H.M., 2017. Phosphomannosylation and the functional analysis of the extended *Candida albicans MNN4*-like gene family. Front Microbiol 8. https://doi.org/10.3389/fmicb.2017.02156.

Gow, N.A.R., Netea, M.G., Munro, C.A., Ferwerda, G., Bates, S., Mora-Montes, H.M., et al., 2007. Immune recognition of *Candida albicans* beta-glucan by dectin-1. J. Infect. Dis. 196, 1565–1571.

Graham, L.M., Tsoni, S.V., Willment, J.A., Williams, D.L., Taylor, P.R., Gordon, S., et al., 2006. Soluble Dectin-1 as a tool to detect beta-glucans. J Immunol Methods 314, 164–169.

Graninger, M., Nidetzky, B., Heinrichs, D.E., Whitfield, C., Messner, P., 1999. Characterization of dTDP-4-dehydrorhamnose 3,5-epimerase and dTDP-4-dehydrorhamnose reductase, required for dTDP-L-rhamnose biosynthesis in *Salmonella enterica* serovar Typhimurium LT2. J Biol Chem 274 (35), 25069–25077.

Heinsbroek, S.E.M., Taylor, P.R., Martinez, F.O., Martinez-Pomares, L., Brown, G.D., Gordon, S., Filler, S.G., 2008. Stage-specific sampling by pattern recognition receptors during *Candida albicans* phagocytosis. PLOS Pathog 4 (11), e1000218.

Hernández-Chávez, M.J., Clavijo-Giraldo, D.M., Novák, Á., Lozoya-Pérez, N.E., Martínez-Álvarez, J.A., Salinas-Marín, R., Hernández, N.V., Martínez-Duncker, I., Gácser, A., Mora-Montes, H.M., 2019. Role of protein mannosylation in the *Candida tropicalis*-

host interaction. Front Microbiol 10. https://doi.org/10.3389/fmicb.2019.0274310.3389/fmicb.2019.02743.s001.

M.J. Hernández-Chávez B. Franco D.M. Clavijo-Giraldo N.V. Hernández E. Estrada-Mata H.M. Mora-Montes Role of protein phosphomannosylation in the Candida tropicalis-macrophage interaction 18 5 2018 2018 10.1093/femsyr/foy053.

Hobson, R.P., Munro, C.A., Bates, S., MacCallum, D.M., Cutler, J.E., Heinsbroek, S.E.M., Brown, G.D., Odds, F.C., Gow, N.A.R., 2004. Loss of cell wall mannosylphosphate in *Candida albicans* does not influence macrophage recognition. J Biol Chem 279 (38), 39628–39635.

Jellmayer, J.A., Ferreira, L.S., Manente, F.A., Gonçalves, A.C., Polesi, M.C., Batista-Duharte, A., Carlos, I.Z., 2017. Dectin-1 expression by macrophages and related antifungal mechanisms in a murine model of *Sporothrix schenckii sensu stricto* systemic infection. Microb. Pathog. 110, 78–84.

Jeng, A., Sakota, V., Li, Z., Datta, V., Beall, B., Nizet, V., 2003. Molecular genetic analysis of a group A *Streptococcus* operon encoding serum opacity factor and a novel fibronectin-binding protein, SfbX. J. Bacteriol. 185 (4), 1208–1217.

Kavanagh, K.L., Jörnvall, H., Persson, B., Oppermann, U., 2008. Medium- and short-chain dehydrogenase/reductase gene and protein families : the SDR superfamily: functional and structural diversity within a family of metabolic and regulatory enzymes. Cell Mol Life Sci 65 (24), 3895–3906.

Koga, T., Asakawa, H., Okahashi, N., Takahashi, I., 1989. Effect of subculturing on expression of a cell-surface protein antigen by *Streptococcus mutans*. J. Gen. Microbiol. 135, 3199–3207.

Latgé, J.-P., Beauvais, A., Chamilos, G., 2017. The cell wall of the human fungal pathogen *Aspergillus fumigatus*: biosynthesis, organization, immune response, and virulence. Ann Rev Microbiol 71 (1), 99–116.

Livak, K.J., Schmittgen, T.D., 2001. Analysis of relative gene expression data using real-time quantitative PCR and the 2(-Delta Delta C(T)) Method. Methods 25, 402–408.

Lloyd, K.O. and Bitoon, M.A. (1971). Isolation and purification of a peptido-rhamnomannan from the yeast form of Sporothrix schenckii. Structural and immunochemical studies. Journal of immunology (Baltimore, Md. : 1950) 107, 663-671.

Lopes-Bezerra, L.M., 2011. *Sporothrix schenckii* cell wall peptidorhamnomannans. Front Microbiol 2, 243.

Lopes-Bezerra, L.M., Mora-Montes, H.M., Zhang, Y., Niño-Vega, G.A., Rodrigues, A.M., de Camargo, Z.P., de Hoog, S., 2018a. Sporotrichosis between 1898 and 2017: The evolution of knowledge on a changeable disease and on emerging etiological agents. Med Mycol 56 (suppl 1), 126–143. https://doi.org/10.1093/mmy/myx103.

Lopes-Bezerra, L.M., Walker, L.A., Niño-Vega, G., Mora-Montes, H.M., Neves, G.W.P., Villalobos-Duno, H., Barreto, L., Garcia, K., Franco, B., Martínez-Álvarez, J.A., Munro, C.A., Gow, N.A.R., Reynolds, T.B., 2018b. Cell walls of the dimorphic fungal pathogens *Sporothrix schenckii* and *Sporothrix brasiliensis* exhibit bilaminate structures and sloughing of extensive and intact layers. PLoS Negl Trop Dis 12 (3), e0006169.

Lozoya-Perez, N.E., Casas-Flores, S., de Almeida, J.R.F., Martinez-Alvarez, J.A., Lopez-Ramirez, L.A., Jannuzzi, G.P., et al., 2019. Silencing of *OCH1* unveils the role of *Sporothrix schenckii N*-linked glycans during the host-fungus interaction. Infect Drug Resist 12, 67–85.

Lozoya-Pérez, N.E., Casas-Flores, S., Martínez-Álvarez, J.A., López-Ramírez, L.A., Lopes-Bezerra, L.M., Franco, B., Mora-Montes, H.M., 2018. Generation of *Sporothrix schenckii* mutants expressing the green fluorescent protein suitable for the study of host-fungus interaction. Fungal Biol. 122 (11), 1023–1030.

Lozoya-Pérez, N.E., Clavijo-Giraldo, D.M., Martínez-Duncker, I., García-Carnero, L.C., López-Ramírez, L.A., Niño-Vega, G.A., Mora-Montes, H.M., 2020. Influences of the culturing media in the virulence and cell wall of *Sporothrix schenckii, Sporothrix brasiliensis*, and *Sporothrix globosa*. J Fungi (Basel) 6 (4), 323. https://doi.org/10.3390/jof6040323.

Ma, L., Salas, O., Bowler, K., Oren-Young, L., Bar-Peled, M., Sharon, A., 2017. Genetic alteration of UDP-rhamnose metabolism in *Botrytis cinerea* leads to the accumulation of UDP-KDG that adversely affects development and pathogenicity. Mol Plant Pathol 18 (2), 263–275.

Ma, Y., Pan, F., McNeil, M., 2002. Formation of dTDP-rhamnose is essential for growth of Mycobacteria. J. Bacteriol. 184 (12), 3392–3395.

Macêdo-Sales, P.A., Souza, L.O.P., Della-Terra, P.P., Lozoya-Pérez, N.E., Machado, R.L. D., Rocha, E.M.d.S.d., Lopes-Bezerra, L.M., Guimarães, A.J., Rodrigues, A.M., Mora-Montes, H.M., Santos, A.L.S.D., Baptista, A.R.d.S., 2020. Coinfection of domestic felines by distinct *Sporothrix brasiliensis* in the Brazilian sporotrichosis hyperendemic area. Fungal Genet Biol 140, 103397. https://doi.org/10.1016/j.fgb.2020.103397.

Marakalala, M.J., Vautier, S., Potrykus, J., Walker, L.A., Shepardson, K.M., Hopke, A., et al., 2013. Differential adaptation of *Candida albicans in vivo* modulates immune recognition by dectin-1. PLoS Pathog 9, e1003315.

Martínez-Álvarez, J.A., García-Carnero, L.C., Kubitschek-Barreira, P.H., Lozoya-Pérez, N. E., Belmonte-Vázquez, J.L., de Almeida, J.RF., J Gómez-Infante, A.J., Curty, N., Villagómez-Castro, J.C., Peña-Cabrera, E., Martínez-Duncker, I., Almeida, S.R., Lopes-Bezerra, L.M., Mora-Montes, H.M., 2019. Analysis of some immunogenic properties of the recombinant *Sporothrix schenckii* Gp70 expressed in *Escherichia coli*. Future microbiology 14 (5), 397–410.

Martínez-Álvarez, J.A., Pérez-García, L.A., Flores-Carreón, A., Mora-Montes, H.M., 2014. The immune response against *Candida* spp. and *Sporothrix schenckii*. Rev Iberoam Micol 31 (1), 62–66.

Martinez-Alvarez, J.A., Perez-Garcia, L.A., Mellado-Mojica, E., Lopez, M.G., Martinez-Duncker, I., Lopes-Bezerra, L.M., Mora-Montes, H.M., 2017. *Sporothrix schenckii sensu stricto* and *Sporothrix brasiliensis* are differentially recognized by human peripheral blood mononuclear cells. Front Microbiol 8, 843.

Martinez, V., Ingwers, M., Smith, J., Glushka, J., Yang, T., Bar-Peled, M., 2012. Biosynthesis of UDP-4-keto-6-deoxyglucose and UDP-rhamnose in pathogenic fungi *Magnaporthe grisea* and *Botryotinia fuckeliana*. J Biol Chem 287 (2), 879–892.

Mistou, M.-Y., Sutcliffe, I.C., van Sorge, N.M., Bitter, W., 2016. Bacterial glycobiology: rhamnose-containing cell wall polysaccharides in Gram-positive bacteria. FEMS Microbiol Rev 40 (4), 464–479.

Mora-Montes, H.M., Bates, S., Netea, M.G., Castillo, L., Brand, A., Buurman, E.T., Díaz-Jiménez, D.F., Jan Kullberg, B., Brown, A.J.P., Odds, F.C., Gow, N.A.R., 2010a. A multifunctional mannosyltransferase family in *Candida albicans* determines cell wall mannan structure and host-fungus interactions. J Biol Chem 285 (16), 12087–12095.

Mora-Montes, H.M., Bates, S., Netea, M.G., Diaz-Jimenez, D.F., Lopez-Romero, E., Zinker, S., et al., 2007. Endoplasmic reticulum alpha-glycosidases of *Candida albicans* are required for N glycosylation, cell wall integrity, and normal host-fungus interaction. Eukaryot Cell 6, 2184–2193.

H.M. Mora-Montes A.d.S. Dantas E. Trujillo-Esquivel A.R. de Souza Baptista L.M. Lopes-Bezerra C. Munro 15 6 2015 fov065 10.1093/femsyr/fov065.

Mora-Montes, H.M., McKenzie, C., Bain, J.M., Lewis, L.E., Erwig, L.P., Gow, N.A., 2012. Interactions between macrophages and cell wall oligosaccharides of *Candida albicans*. Methods Mol Biol 845, 247–260.

Mora-Montes, H.M., Netea, M.G., Ferwerda, G., Lenardon, M.D., Brown, G.D., Mistry, A. R., Kullberg, B.J., O'Callaghan, C.A., Sheth, C.C., Odds, F.C., Brown, A.J.P., Munro, C.A., Gow, N.A., Deepe, G.S., 2011. Recognition and blocking of innate immunity cells by *Candida albicans* chitin. Infect Immun 79 (5), 1961–1970.

Mora-Montes, H.M., Robledo-Ortiz, C.I., Gonzalez-Sanchez, L.C., Lopez-Esparza, A., Lopez-Romero, E., Flores-Carreon, A., 2010b. Purification and biochemical characterisation of endoplasmic reticulum alpha1,2-mannosidase from *Sporothrix schenckii*. Mem Inst Oswaldo Cruz 105, 79–85.

Nakayashiki, H., Hanada, S., Quoc, N.B., Kadotani, N., Tosa, Y., Mayama, S., 2005. RNA silencing as a tool for exploring gene function in ascomycete fungi. Fungal Genet. Biol. 42 (4), 275–283.

Navarro-Arias, M.J., Defosse, T.A., Dementhon, K., Csonka, K., Mellado-Mojica, E., Dias Valério, A., González-Hernández, R.J., Courdavault, V., Clastre, M., Hernández, N. V., Pérez-García, L.A., Singh, D.K., Vizler, C., Gácser, A., Almeida, R.S., Noël, T., López, M.G., Papon, N., Mora-Montes, H.M., 2016. Disruption of protein mannosylation affects *Candida guilliermondii* cell wall, immune sensing, and virulence. Front Microbiol 7. https://doi.org/10.3389/fmicb.2016.01951.

Negrini, T.d.C., Ferreira, L.S., Alegranci, P., Arthur, R.A., Sundfeld, P.P., Maia, D.C.G., Spolidorio, L.C., Carlos, I.Z., 2013. Role of TLR-2 and fungal surface antigens on innate immune response against *Sporothrix schenckii*. Immunol Investigat 42 (1), 36–48.

Netea, M.G., Brown, G.D., Kullberg, B.J., Gow, N.A.R., 2008. An integrated model of the recognition of *Candida albicans* by the innate immune system. Nat. Rev. Microbiol. 6 (1), 67–78.

Netea, M.G., Gow, N.A., Munro, C.A., Bates, S., Collins, C., Ferwerda, G., et al., 2006. Immune sensing of *Candida albicans* requires cooperative recognition of mannans and glucans by lectin and Toll-like receptors. J Clin Invest 116, 1642–1650.

Pérez-García, L.A., Csonka, K., Flores-Carreón, A., Estrada-Mata, E., Mellado-Mojica, E., Németh, T., López-Ramírez, L.A., Toth, R., López, M.G., Vizler, C., Marton, A., Tóth, A., Nosanchuk, J.D., Gácser, A., Mora-Montes, H.M., 2016. Role of protein glycosylation in *Candida parapsilosis* cell wall integrity and host interaction. Front Microbiol 7. https://doi.org/10.3389/fmicb.2016.00306.

Pinto, M.R., de Sá, A.C.M., Limongi, C.L., Rozental, S., Santos, A.L.S., Barreto-Bergter, E., 2004. Involvement of peptidorhamnomannan in the interaction of *Pseudallescheria boydii* and HEp2 cells. Microbes Infect 6 (14), 1259–1267.

Pinto, M.R., Mulloy, B., Haido, R.M.T., Travassos, L.R., Barreto Bergter, E., 2001. A peptidorhamnomannan from the mycelium of *Pseudallescheria boydii* is a potential diagnostic antigen of this emerging human pathogen. Microbiology 147, 1499–1506.

Reid, D.M., Gow, N.AR., Brown, G.D., 2009. Pattern recognition: recent insights from Dectin-1. Curr Opin Immunol 21 (1), 30–37.

Robledo-Ortiz, C.I., Flores-Carreón, A., Hernández-Cervantes, A., Álvarez-Vargas, A., Lee, K.K., Díaz-Jiménez, D.F., Munro, C.A., Cano-Canchola, C., Mora-Montes, H.M., 2012. Isolation and functional characterization of *Sporothrix schenckii ROT2*, the encoding gene for the endoplasmic reticulum glucosidase II. Fungal Biol 116 (8), 910–918.

Rodriguez-Caban, J., Gonzalez-Velazquez, W., Perez-Sanchez, L., Gonzalez-Mendez, R., Valle, N.R.–D., 2011. Calcium/calmodulin kinase1 and its relation to thermotolerance and HSP90 in *Sporothrix schenckii*: an RNAi and yeast two-hybrid study. BMC Microbiol. 11, 162.

Santhanam, P., Boshoven, J.C., Salas, O., Bowler, K., Islam, M.T., Saber, M.K., van den Berg, G.C.M., Bar-Peled, M., Thomma, B.P.H.J., 2017. Rhamnose synthase activity is required for pathogenicity of the vascular wilt fungus *Verticillium dahliae*. Mol. Plant Pathol 18 (3), 347–362.

Sassá, M.F., Ferreira, L.S., de Abreu Ribeiro, L.C., Carlos, I.Z., 2012. Immune response against *Sporothrix schenckii* in TLR-4-deficient mice. Mycopathologia 174 (1), 21–30.

Taylor, P.R., Brown, G.D., Reid, D.M., Willment, J.A., Martinez-Pomares, L., Gordon, S. and Wong, S.Y. (2002). The beta-glucan receptor, dectin-1, is predominantly expressed on the surface of cells of the monocyte/macrophage and neutrophil lineages. Journal of immunology (Baltimore, Md. : 1950) 169, 3876-3882.

Teixeira, M.M., de Almeida, L.GP., Kubitschek-Barreira, P., Alves, F.L., Kioshima, Érika. S., Abadio, A.KR., Fernandes, L., Derengowski, L.S., Ferreira, K.S., Souza, R.C., Ruiz, J.C., de Andrade, N.C., Paes, H.C., Nicola, André.M., Albuquerque, P., Gerber, A.L., Martins, V.P., Peconick, L.DF., Neto, A., Chaucanez, C.B., Silva, Patrícia.A., Cunha, O.L., de Oliveira, F.FM., dos Santos, Tayná.C., Barros, A. LN., Soares, M.A., de Oliveira, L.M., Marini, M.M., Villalobos-Duno, Héctor, Cunha, M.ML., de Hoog, S., da Silveira, José.F., Henrissat, B., Niño-Vega, G.A.,

Cisalpino, Patrícia.S., Mora-Montes, Héctor.M., Almeida, S.R., Stajich, J.E., Lopes-Bezerra, L.M., Vasconcelos, A.TR., Felipe, M.SS., 2014. Comparative genomics of the major fungal agents of human and animal Sporotrichosis: *Sporothrix schenckii* and *Sporothrix brasiliensis*. BMC Genomics 15 (1), 943. https://doi.org/10.1186/1471-2164-15-943.

Pedro Antônio Castelo Teixeira Rafaela Alves de Castro Rosana Cícera Nascimento Guy Tronchin Armando Pérez Torres Márcia Lazéra Sandro Rogério de Almeida Jean-Philippe Bouchara Carla Veronica Loureiro y Penha Leila M. Lopes-Bezerra Cell surface expression of adhesins for fibronectin correlates with virulence in Sporothrix schenckii 155 11 2009 3730 3738.

Teng, F., Jacques-Palaz, K.D., Weinstock, G.M., Murray, B.E., 2002. Evidence that the enterococcal polysaccharide antigen gene (epa) cluster is widespread in *Enterococcus faecalis* and influences resistance to phagocytic killing of *E. faecalis*. Infect Immun 70 (4), 2010–2015.

Trujillo-Esquivel, E., Franco, B., Flores-Martínez, A., Ponce-Noyola, P., Mora-Montes, Héctor.M., 2016. Purification of Single-Stranded cDNA Based on RNA Degradation Treatment and Adsorption Chromatography. Nucleosides Nucleotides Nucleic Acids 35 (8), 404–409.

Trujillo-Esquivel, E., Martinez-Alvarez, J.A., Clavijo-Giraldo, D.M., Hernandez, N.V., Flores-Martinez, A., Ponce-Noyola, P., Mora-Montes, H.M., 2017. The *Sporothrix schenckii* gene encoding for the ribosomal protein L6 has constitutive and stable expression and works as an endogenous control in gene expression analysis. Front Microbiol 8, 1676.

Valiante, V., 2017. The cell wall integrity signaling pathway and its involvement in secondary metabolite production. J Fungi (Basel) 3 (4), 68. https://doi.org/10.3390/jof3040068.

van der Beek, S.L., Le Breton, Y., Ferenbach, A.T., Chapman, R.N., van Aalten, D.M.F., Navratilova, I., Boons, G.-J., McIver, K.S., van Sorge, N.M., Dorfmueller, H.C., 2015. GacA is essential for Group A *Streptococcus* and defines a new class of monomeric dTDP-4-dehydrorhamnose reductases (RmlD). Mol. Microbiol. 98 (5), 946–962.

Wagstaff, B.A., Rejzek, M., Kuhaudomlarp, S., Hill, L., Mascia, I., Nepogodiev, S.A., Dorfmueller, H.C., Field, R.A., 2019. Discovery of an RmlC/D fusion protein in the microalga *Prymnesium parvum* and its implications for NDP-β-L-rhamnose biosynthesis in microalgae. J Biol Chem 294 (23), 9172–9185.

Watt, G., Leoff, C., Harper, A.D., Bar-Peled, M., 2004. A bifunctional 3,5-epimerase/4-keto reductase for nucleotide-rhamnose synthesis in Arabidopsis. Plant Physiol. 134 (4), 1337–1346.